An FE-based orientation averaging model for elasto-plastic behavior of short fiber composites

International Journal of Mechanical Sciences 219 (2022) 107097

Contents lists available at ScienceDirect

International Journal of Mechanical Sciences

journal homepage: www.elsevier.com/locate/ijmecsci

An FE-based orientation averaging model for elasto-plastic behavior of short fiber composites

S.M. Mirkhalaf [a,b,*], T.J.H. van Beurden [b,c], M. Ekh [b], F. Larsson [b], M. Fagerström [b]

[a] Department of Physics, University of Gothenburg, Gothenburg, Sweden
[b] Division of Material and Computational Mechanics, Department of Industrial and Materials Science, Chalmers University of Technology, Gothenburg, Sweden
[c] Department of Mechanical Engineering, Eindhoven University of Technology, Eindhoven, Netherlands

ARTICLE INFO

Keywords:
Short fiber reinforced composites
Mechanical behavior
Micro-mechanical modeling
Orientation averaging
Finite element analysis

ABSTRACT

A new micro-mechanical model for predicting the non-linear elasto-plastic behavior of short fiber reinforced composites is presented. The model is developed based on a two-step *Orientation Averaging* method, and is capable of accommodating a wide variety of micro-structural parameters. In the first step, *Finite Element Analyses* are performed on a unit cell (single fiber surrounded by matrix). Then, the unit cell response is up-scaled by calibrating its response to an elasto-plastic *surrogate constitutive model*. In a subsequent second homogenization step, a self-consistent interaction scheme is proposed. The predictive capability of the resulting two-step homogenization scheme is then evaluated, next to versions that adopt more traditional averaging schemes (Voigt and Reuss, providing upper and lower bounds, respectively), through comparisons to experiments and direct numerical simulations of realistic Representative Volume Elements. Results show that the model gives fairly good predictions. It is emphasized that the model is capable of accommodating any desired fiber orientation distribution, very large ranges of fiber aspect ratios and fiber volume fractions. Also, the model is computationally very efficient compared to the RVE computational homogenization approach, and thus, it could be conveniently used in applications possessing different fiber orientations at different points of a component.

1. Introduction

Short Fiber Reinforced Composites (SFRCs) possess interesting mechanical properties compared to neat matrix materials. Also, SFRC parts with complicated geometries can be produced via injection molding [1]. Thus, SFRCs are obtaining rising popularity by different industrial sectors such as car industry. In order to predict the performance of SFRC parts in extreme cases (such as crash) it is required to know not only the elastic behavior, but also the plastic response. To do so accurately and based on actual micro-structural characteristics, using micro-mechanical models is inevitable [2]. As a result, a large number of studies have been conducted on this topic, see e.g. [2–6].

Micromechanical modeling approaches of different materials could be traditionally categorized to two main classes of models: *mean-field* and *full-field* models. Mean-field models assume average strain and stress in each of the individual phases of a micro-structure. Typically, explicit analytical relations are obtained for the average response of the micro-structure. A large number of mean-field models are developed for different classes of materials, see e.g. [3,7] for SFRCs, [8] for semi-crystalline polymers, and [9] for an overview of different methods for unidirectional composites. Mean-field models are typically developed based on classical mean-field theories such as those by Eshelby [10], Hashin and Shtrikman [11,12], Hill [13], Budiansky [14], and Mori–Tanaka [15], among others. An interested reader in mean-field modeling of SFRCs, is referred to a recent work by Hessman et al. [16].

Full-field models, contrary to the mean-field models, account for microscopic fields at different microscopic points. Equilibrium equations are solved using different numerical techniques such as Finite Element Method [17–20] or Fast Fourier Transform [21,22]. For full-field analysis, it is required to generate realistic Representative Volume Elements (RVEs) which are representative for the material micro-structure. If the constituents are modeled accurately, this method is very accurate. But it is not always applicable. First of all, generating realistic numerical RVEs (which mimic the actual material micro-structure) is in some cases (e.g. high aspect ratio of fibers and high fiber volume fractions) very challenging [23–25]. Different authors have developed methods for generating microstructural samples for SFRCs, see e.g. [23,26–29].

* Corresponding author at: Department of Physics, University of Gothenburg, Gothenburg, Sweden.
E-mail address: mohsen.mirkhalaf@physics.gu.se (S.M. Mirkhalaf).

https://doi.org/10.1016/j.ijmecsci.2022.107097
Received 31 May 2021; Received in revised form 18 January 2022; Accepted 18 January 2022
Available online 3 February 2022

However, it is still challenging to generate RVEs with variety of arbitrary microstructural features. Another challenge of full-field analysis is the computational cost of this approach, in particular, when coupled multi-scale FE^2 simulations are needed. Hence, it is needed to develop other micro-mechanical models to overcome the limitations of this approach. For comparisons of different micro-mechanical approaches and applications to SFRCs, an interested reader is referred to [30–33]. More recently, data-driven approaches are also employed for modeling the mechanical behavior of SFRCs [34,35].

Through the last decades, different studies have been devoted to developing micro-mechanical models to predict inelastic behavior of SFRCs, see e.g. [1,36,37]. Doghri and Tinel [36] developed a mean-field micro-mechanical model for elasto-plastic behavior of non-uniformly distributed fiber reinforced materials. Two homogenization steps were defined in the mean-field approach [36]. First, a Representative Volume Element is decomposed to so-called pseudo-grains (containing identical and aligned inclusions), and each pseudo-grain is homogenized based on Mori–Tanaka method [15]. In the second step, homogenization is performed over all pseudo-grains using a Voigt assumption. The model was further extended by Kammoun et al. [37] and Kammoun et al. [1] to incorporate failure and damage.

In this study, a two-step micro-mechanical model based on numerical and analytical homogenization is presented for describing the elasto-plastic behavior of SFRCs. The model is developed on an *Orientation Averaging* platform following the study by Advani and Tucker [38]. The model is an extension of the previous study on the elastic properties of SFRCs [39] to non-linear elasto-plastic deformation regime. Two configurations, namely global (at the composite level) and local (at the fibers level) are distinguished. At the local configuration, Unit Cells (UCs) are defined as single fibers surrounded by matrix material. Elasto-plastic FE calculations are performed on a UC and then the unit cell response is up-scaled by calibrating a *surrogate constitutive model* against the FE results. The calibrated surrogate model (representing the UC behavior) is then, in a second homogenization step, used within the averaging framework to predict composite behavior. As a complement to interaction schemes traditionally used in the literature, i.e. Voigt and Reuss that provide upper and lower bounds, also a self-consistent assumption is proposed and evaluated in this paper. Obtained numerical results show that the proposed two-step homogenization model gives fairly good predictions, often in favor of the self-consistent interaction scheme. This implies that using this approach, SFRCs with a broad range of micro-structural parameters such as high fiber aspect ratios, high fiber volume fractions, and any desired fiber orientation distributions can be modeled in an efficient way with an acceptable accuracy.

The remaining of this paper is structured as follows. Section 2 describes the Orientation Averaging framework which is in fact the platform of the proposed model. Section 3 explains how strain state of each UC is obtained as a function of macroscopic strain state, and considering different global–local interactions, namely Voigt, Reuss and self-consistent assumptions. Section 4 details the surrogate constitutive model which will be calibrated based on the FE calculations of a UC, and will be used to calculate each UC stress in each load increment. Then, the implementation of the model, in an incremental scheme, is described in Section 5. In Section 6, first, the suitability of the proposed UC structure is confirmed through comparisons to unidirectional RVEs. Then, numerical examples are presented, and comparisons are conducted to experimental results (taken from literature), as well as direct numerical simulations of realistic RVEs. Finally, Section 7 summarizes the conclusions of this study, and discusses the advantages of the presented model.

2. Orientation Averaging framework

In this section, the Orientation Averaging framework, which is the basis of the presented model, is described. First, an RVE is divided to UCs (each UC composed of a single fiber surrounded by matrix material). In this study, and RVE is an aggregate of UCs. A global configuration with a global coordinate system (at the composite level), and a local configuration with a local coordinate system (at the UC level) are considered. A schematic representation of a Unit Cell, and the two aforementioned configurations are depicted in Fig. 1.

The transformation (rotation) from the global (composite) configuration system to the local (UC) configuration is defined by $\mathbf{R}$:

$$\mathbf{e}_i^L = \mathbf{R} \cdot \mathbf{e}_i, \tag{1}$$

where, $\mathbf{e}_i$ and $\mathbf{e}_i^L$ indicate the global and local orthonormal base vectors, respectively. The orientation of a fiber ($\mathbf{p}$) is defined by two angles (spherical coordinates) [38], as it is shown in Fig. 2. The matrix representation of the rotation tensor, using ϕ and θ, is given by

$$\mathbf{R}(\mathbf{p}) = \mathbf{R}(\mathbf{p}(\phi,\theta)) = \begin{bmatrix} \cos(\phi)\sin(\theta) & -\sin(\phi) & -\cos(\phi)\cos(\theta) \\ \sin(\phi)\sin(\theta) & \cos(\phi) & -\sin(\phi)\cos(\theta) \\ \cos(\theta) & 0 & \sin(\theta) \end{bmatrix}. \tag{2}$$

This rotation tensor is obtained by considering the local direction 1 as the fiber direction. In other words, $\mathbf{e}_1^L$ is a unit vector representing the fiber orientation ($\mathbf{e}_1^L = \mathbf{p}$). To obtain the rotation tensor, initially, the global configuration is rotated by an angle of $-(\frac{\pi}{2} - \theta)$ around axis-2. Secondly, it is rotated by an angle of ϕ around axis-3.

In this method, it is needed to first obtain each UC mechanical response. Different approaches could be used for that purpose (see [9] for an overview of stiffness and strength predictions). In this study, FE simulations are conducted to calculate the UC response, and then a surrogate constitutive model is developed and calibrated to replace the FE calculations. Once the UC stress components at the local configuration ($\boldsymbol{\sigma}_U^L$) are known, the UC stress components at the global configuration ($\boldsymbol{\sigma}_U$) are obtained (simply by a coordinate transformation) by

$$\boldsymbol{\sigma}_U = \mathbf{R}^T(\mathbf{p}) \cdot \boldsymbol{\sigma}_U^L \cdot \mathbf{R}(\mathbf{p}) = \left[\mathbf{R}^T(\mathbf{p}) \,\overline{\otimes}\, \mathbf{R}^T(\mathbf{p})\right] : \boldsymbol{\sigma}_U^L. \tag{3}$$

Note that $\boldsymbol{\sigma}_U$ and $\boldsymbol{\sigma}_U^L$ are both representing the same stress tensor, only with components at *different coordinate systems*. The operator $\overline{\otimes}$ represents a non-standard open product.[1] By weighted integration over the unit sphere, the volume averaged composite stress becomes:

$$\boldsymbol{\sigma}_C = \oint \left[\mathbf{R}^T(\mathbf{p}) \,\overline{\otimes}\, \mathbf{R}^T(\mathbf{p})\right] : \boldsymbol{\sigma}_U^L \; \psi(\mathbf{p}) \mathrm{d}\mathbf{p}, \tag{4}$$

where $\boldsymbol{\sigma}_C$ are the components of the composite stress in the global coordinate system, and $\psi(\mathbf{p})$ is the probability distribution function of orientation [38]. By assuming no rotation of the fibers during deformation, the rate form of Eq. (4) reads:

$$\dot{\boldsymbol{\sigma}}_C = \oint \left[\mathbf{R}^T(\mathbf{p}) \,\overline{\otimes}\, \mathbf{R}^T(\mathbf{p})\right] : \dot{\boldsymbol{\sigma}}_U^L \; \psi(\mathbf{p}) \mathrm{d}\mathbf{p}. \tag{5}$$

As a result, the incremental stress is obtained as

$$\Delta\boldsymbol{\sigma}_C = \oint \left[\mathbf{R}^T(\mathbf{p}) \,\overline{\otimes}\, \mathbf{R}^T(\mathbf{p})\right] : \Delta\boldsymbol{\sigma}_U^L \; \psi(\mathbf{p}) \mathrm{d}\mathbf{p}, \tag{6}$$

where $\Delta\boldsymbol{\sigma}_U^L$ is the incremental UC stress at the local configuration. It should be emphasized that we are assuming small strains and thus, the fiber orientations are considered unchanged during the deformation.

3. Strain state of each Unit Cell

To determine the incremental update of the UC stress ($\Delta\boldsymbol{\sigma}_U^L$), it is required to obtain strain state of each UC ($\boldsymbol{\varepsilon}_U^L$) considering its own orientation and also the interaction assumption. In this study, three different *global–local* interactions, namely Voigt, Reuss and self-consistent assumptions are used. These interactions determine microscopic strain state (for UCs) considering the macroscopic (composite) strain state.

[1] The index notation for the non-standard open product ($\overline{\otimes}$) is given by $(\mathbf{A}\overline{\otimes}\mathbf{B})_{ijkl} = A_{ik}B_{jl}$.

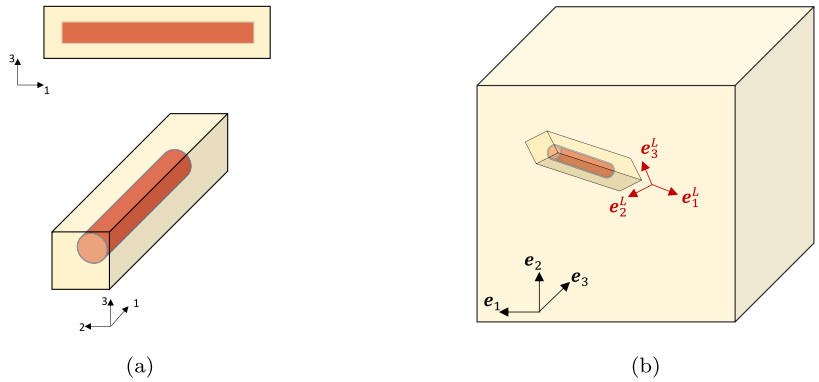

Fig. 1. (a): A schematic representation of a Unit Cell and its corresponding local coordinate system, (b): A schematic representation of the global and local coordinate systems at the composite and UC levels. These coordinate systems are defined for the orientation averaging framework in order to perform the required rotations between the two coordinate systems.

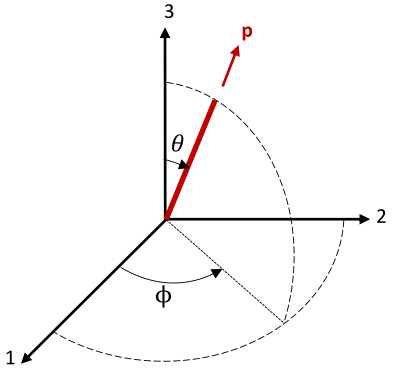

Fig. 2. Orientation of a fiber can be described using two angles considering spherical coordinates, as shown by ϕ and θ. The fiber orientation distribution function in a material point is defined using the two angles. The second order rotation tensor (for each fiber orientation) is then obtained as a function of these two angles.

3.1. Voigt interaction

The Voigt assumption implies that interacting components experience the same strain at the global configuration:

$$\Delta\boldsymbol{\varepsilon}_{\mathrm{U}} = \Delta\boldsymbol{\varepsilon}_{\mathrm{C}}, \tag{7}$$

where $\Delta\boldsymbol{\varepsilon}_{\mathrm{C}}$ and $\Delta\boldsymbol{\varepsilon}_{\mathrm{U}}$ are the incremental composite strain and incremental UC strain at the global configuration, respectively. In order to obtain the local stress of each UC, the local components of the strain increment of each UC are computed as

$$\Delta\boldsymbol{\varepsilon}_U^L = \mathbf{R}(\mathbf{p}) \cdot \Delta\boldsymbol{\varepsilon}_C \cdot \mathbf{R}^T(\mathbf{p}) = \left[\mathbf{R}(\mathbf{p}) \,\overline{\otimes}\, \mathbf{R}(\mathbf{p})\right] : \Delta\boldsymbol{\varepsilon}_C. \tag{8}$$

Note that, $\boldsymbol{\varepsilon}_U$ and $\boldsymbol{\varepsilon}_U^L$ are representing the same tensor, *with components at different configurations* (similarly to stress components). The Voigt assumption gives the upper bound of stiffness predictions.

3.2. Reuss interaction

The Reuss assumption means that all UCs experience the same stress:

$$\boldsymbol{\sigma}_U = \boldsymbol{\sigma}_C. \tag{9}$$

Thus, the local components of the UC stress are given by

$$\Delta\boldsymbol{\sigma}_U^L = \mathbf{R}(\mathbf{p}) \cdot \Delta\boldsymbol{\sigma}_U \cdot \mathbf{R}^T(\mathbf{p}) = \left[\mathbf{R}(\mathbf{p}) \,\overline{\otimes}\, \mathbf{R}(\mathbf{p})\right] : \Delta\boldsymbol{\sigma}_U. \tag{10}$$

Once the incremental UC stress components at the local coordinate system ($\Delta\boldsymbol{\sigma}_U^L$) is known, it is possible to obtain the incremental local components of the UC strain as

$$\Delta\boldsymbol{\varepsilon}_U^L = (\mathbb{C}_U^L)^{-1} : \Delta\boldsymbol{\sigma}_U^L, \tag{11}$$

where $\mathbb{C}_U^L$ is the UC stiffness tensor at the local coordinate system. The Reuss assumption gives the lower bound of stiffness predictions.

3.3. Self-consistent interaction

With the Voigt and Reuss interactions, the upper and lower bounds of stiffness are obtained, respectively. Uniform strain (Voigt) and uniform stress (Reuss) assumptions are typically strong assumptions which, in some cases, may lead to unrealistic results. This is partly explained by the fact that both these interaction schemes neglect to account for interaction between neighboring fibers. Therefore, a self-consistent assumption is used to develop an additional interaction rule in which fiber interaction is implicitly accounted for. Thereby, it will also result in an intermediate approach between the Voigt and Reuss assumptions. Using the self-consistent assumption means that each of the unit cells are embedded in an *equivalent homogeneous medium*. In other words, the state of each UC in the aggregate[2] is equivalent to the state of the UC embedded in a matrix with properties equivalent to the whole aggregate. Using this interaction, the UC incremental strain is obtained by (see [39] for details):

$$\Delta\boldsymbol{\varepsilon}_U = \left[\mathbb{I} + \mathbb{E} : \left(\left[\mathbb{C}_C^{SC}\right]^{-1} : \mathbb{C}_U - \mathbb{I}\right)\right]^{-1} : \Delta\boldsymbol{\varepsilon}_C, \tag{12}$$

where $\mathbb{I}$ is the fourth order identity tensor, $\mathbb{E}$ is the fourth order Eshelby tensor which is a function of stiffness tensor, $\mathbb{C}_C^{SC}$ is the composite stiffness tensor using the self-consistent assumption, and $\mathbb{C}_U$ is the UC stiffness tensor at the global coordinate system. In Eq. (12), it is needed to have the composite stiffness, which is given by (see [39] for details):

$$\mathbb{C}_C^{SC} = \oint \mathbb{C}_U : \left[\mathbb{I} + \mathbb{E} : \left(\left[\mathbb{C}_C^{SC}\right]^{-1} : \mathbb{C}_U - \mathbb{I}\right)\right]^{-1} \psi(\mathbf{p})\mathrm{d}\mathbf{p}. \tag{13}$$

One should note that Eq. (13) does not have an explicit solution, and it has to be solved through an iterative procedure. Mirkhalaf et al. [39] has chosen a fixed point iterative procedure to calculate the composite stiffness. The same procedure is followed here. After the composite stiffness has been obtained, the UC incremental strain is obtained via Eq. (12), whereafter the local incremental UC strain is obtained as

$$\Delta\boldsymbol{\varepsilon}_U^L = \mathbf{R}(\mathbf{p}) \cdot \Delta\boldsymbol{\varepsilon}_U \cdot \mathbf{R}^T(\mathbf{p}) = \left[\mathbf{R}(\mathbf{p}) \,\overline{\otimes}\, \mathbf{R}(\mathbf{p})\right] : \Delta\boldsymbol{\varepsilon}_U. \tag{14}$$

[2] Aggregate refers to a collection of UCs which constitute a macroscopic point.

4. Surrogate constitutive model

To increase the efficiency of the model, we propose to use a surrogate model as a representative of the UC response. The proposed approach is to calibrate a surrogate elasto-plastic model against the unit cell simulation results, and then to use this surrogate model in the orientation averaging procedure. Following this methodology, we will also have an efficient way of obtaining the material tangent behavior at any strain state, without a need for large number of UC simulations. In this study, an elasto-plastic model with a simplified version of transverse isotropic elastic behavior and a simplified transverse isotropic version of the Hill yield criterion is used.

4.1. Elastic behavior

The linear elastic stiffness tensor of the material model is given by

$$\begin{aligned}\mathbb{C}^{\mathrm{e}}_U &= \mathbb{C}^{\mathrm{e,iso}}_U + (C-1)\,(2G+L)\,\mathbf{A} \quad \text{with } \mathbb{C}^{\mathrm{e,iso}}_U \\ &= 2G\mathbb{I} + L\,(\mathbf{I}\otimes\mathbf{I}) \text{ and } \mathbf{A} = \mathbf{p}\otimes\mathbf{p}\end{aligned} \tag{15}$$

where the tensor $\mathbb{C}^{\mathrm{e,iso}}_U$ is the isotropic linear elasticity stiffness tensor, $\mathbf{I}$ is the second order identity tensor, and the scalars G and L are the Lamé parameters. The parameter C is an additional scalar which characterizes the *transverse* isotropic elasticity (in case of $C = 1$, the standard isotropic case is recovered). The elastic stiffness tensor in matrix format, where the Voigt notation is employed, is (when $\mathbf{p} = \mathbf{e}^L_1$) given by

$$\underline{\mathbb{C}}^{\mathrm{e}}_U = \begin{bmatrix} C(2G+L) & L & L & 0 & 0 & 0 \\ L & 2G+L & L & 0 & 0 & 0 \\ L & L & 2G+L & 0 & 0 & 0 \\ 0 & 0 & 0 & G & 0 & 0 \\ 0 & 0 & 0 & 0 & G & 0 \\ 0 & 0 & 0 & 0 & 0 & G \end{bmatrix}. \tag{16}$$

Thus, there are 3 parameters to describe the elasticity of the model: L, G and C.

4.2. Plastic behavior

By following [40] and [41], a mean-stress independent transversely isotropic formulation of Hill's yield function can be formulated as

$$\begin{aligned}\boldsymbol{\Phi}_U(\mathbf{s}_U, \overline{\varepsilon}^p_U) &= (A+2B)\,\mathbf{I} : \mathbf{s}_U + (5A+B-2F)\,\left(\mathbf{A} : \mathbf{s}_U\right)^2 \\ &\quad + 2\,(F-A-2B)\,\mathbf{A} : \mathbf{s}_U^2 - \alpha\left(\overline{\varepsilon}^p_U\right),\end{aligned} \tag{17}$$

where $\mathbf{s}_U$ is the UC deviatoric stress. This expression can after some algebraic manipulations also be expressed as

$$\boldsymbol{\Phi}_U(\mathbf{s}_U, \overline{\varepsilon}^p_U) = \mathbf{s}_U : \mathbb{G}_U : \mathbf{s}_U - \alpha\left(\overline{\varepsilon}^p_U\right) \tag{18}$$

with the fourth order tensor $\mathbb{G}_U$ defined as

$$\mathbb{G}_U = (A+2B)\,\mathbb{I} + (5A+B-2F)\,\mathbf{A}\otimes\mathbf{A} + (F-A-2B)\left[\mathbf{I}\overline{\otimes}\,\mathbf{A} + \mathbf{A}\overline{\otimes}\,\mathbf{I}\right], \tag{19}$$

where $\mathbb{I}$ is the fourth order identity tensor. For the special case that $\mathbf{p} = \mathbf{e}^L_1$ the yield function reads

$$\begin{aligned}\boldsymbol{\Phi}_U &= A\left[\left(\sigma^L_{U,11} - \sigma^L_{U,22}\right)^2 + \left(\sigma^L_{U,11} - \sigma^L_{U,33}\right)^2\right] + B\left(\sigma^L_{U,22} - \sigma^L_{U,33}\right)^2 \\ &\quad + 2\,(A+2B)\left(\sigma^L_{U,23}\right)^2 + 2F\left(\left(\sigma^L_{U,12}\right)^2 + \left(\sigma^L_{U,13}\right)^2\right) - \alpha\left(\overline{\varepsilon}^p_U\right)\end{aligned} \tag{20}$$

From this we can conclude that $2A = 1/(\sigma^{\mathrm{aniso}}_{\mathrm{y}})^2$ where $\sigma^{\mathrm{aniso}}_{\mathrm{y}}$ is the normal yield stress along the fiber direction. Correspondingly, we can identify that $A + B = 1/(\sigma^{\mathrm{iso}}_{\mathrm{y}})^2$ where $\sigma^{\mathrm{iso}}_{\mathrm{y}}$ is the normal yield stress in the isotropic plane. The parameter F can be obtained from a shear yield stress out of the isotropic plane $2F = 1/(\tau^{\mathrm{aniso}}_{\mathrm{y}})^2$. However, it can be noted that the shear yield stress in the isotropic plane is determined from the relation $2(A+2B) = 1/(\tau^{\mathrm{iso}}_{\mathrm{y}})^2$ which shows that $\tau^{\mathrm{iso}}_{\mathrm{y}}$ is not an independent parameter. The reason for this is the assumption of mean-stress independence together with the formulation of Hill's yield surface. In this study we will adopt a simplified version for the shear contributions in (20) by assuming that $F = A + 2B$, i.e.

$$\tau^{\mathrm{aniso}}_{\mathrm{y}} = \tau^{\mathrm{iso}}_{\mathrm{y}} = \frac{1}{\sqrt{2\,(A+2\,B)}} = \frac{\sigma^{\mathrm{aniso}}_{\mathrm{y}}\,\sigma^{\mathrm{iso}}_{\mathrm{y}}}{\sqrt{4\left(\sigma^{\mathrm{aniso}}_{\mathrm{y}}\right)^2 - \left(\sigma^{\mathrm{iso}}_{\mathrm{y}}\right)^2}} \tag{21}$$

By this simplification the choice $\sigma^{\mathrm{aniso}}_{\mathrm{y}} = \sigma^{\mathrm{iso}}_{\mathrm{y}}$ would result in a von Mises yield function.

The function $\alpha(\overline{\varepsilon}^p)$ is the isotropic hardening function, dependent on the accumulated effective plastic strain. In this study, the isotropic hardening function is assumed to be given by

$$\alpha(\overline{\varepsilon}^p_U) = 1 + H_1\overline{\varepsilon}^p_U + H_2(\overline{\varepsilon}^p_U)^2 + H_3(\overline{\varepsilon}^p_U)^3. \tag{22}$$

The parameters H_1, H_2 and H_3 are the hardening parameters. As a result, there are in total 5 material parameters describing the yield and isotropic hardening of the model: 2 parameters for plasticity: ($\sigma^{\mathrm{iso}}_{\mathrm{y}}$ and $\sigma^{\mathrm{aniso}}_{\mathrm{y}}$) and 3 parameters for isotropic hardening: (H_1, H_2 and H_3). We adopt the standard decomposition of the strain into an elastic $\boldsymbol{\varepsilon}^e_U$ and a plastic strain $\boldsymbol{\varepsilon}^p_U$ such that the elasticity relation becomes:

$$\boldsymbol{\sigma}_U = \mathbb{C}^{\mathrm{e}}_U : \boldsymbol{\varepsilon}^e_U = \boldsymbol{\sigma}_U = \mathbb{C}^{\mathrm{e}}_U : \left(\boldsymbol{\varepsilon}_U - \boldsymbol{\varepsilon}^p_U\right). \tag{23}$$

Assuming an associative plasticity model, the rate of plastic strain becomes:

$$\dot{\boldsymbol{\varepsilon}}^p_U = \dot{\lambda}_U \frac{\partial \boldsymbol{\Phi}_U}{\partial \boldsymbol{\sigma}_U} = 2\,\dot{\lambda}_U \mathbb{G}^{\sigma}_U : \boldsymbol{\sigma}_U, \tag{24}$$

where $\dot{\lambda}_U$ is the plastic multiplier which is obtained from complimentary conditions:

$$\dot{\lambda}_U \geq 0, \quad \boldsymbol{\Phi}_U(\boldsymbol{\sigma}_U) \leq 0, \quad \dot{\lambda}_U\,\boldsymbol{\Phi}_U(\boldsymbol{\sigma}_U) = 0. \tag{25}$$

In Eq. (24), $\mathbb{G}^{\sigma}_U$ was introduced which is defined as

$$\mathbb{G}^{\sigma}_U = \mathbb{I}_{\mathrm{dev}} : \mathbb{G}_U : \mathbb{I}_{\mathrm{dev}} \quad \text{with } \mathbb{I}_{\mathrm{dev}} = \mathbb{I} - \frac{1}{3}\mathbf{I}\otimes\mathbf{I}, \tag{26}$$

such that we can formulate the yield function in the total stress $\boldsymbol{\sigma}_U$ as follows:

$$\boldsymbol{\Phi}_U(\boldsymbol{\sigma}_U, \overline{\varepsilon}^p_U) = \boldsymbol{\sigma}_U : \mathbb{G}^{\sigma}_U : \boldsymbol{\sigma}_U - \alpha\left(\overline{\varepsilon}^p_U\right). \tag{27}$$

4.3. Calculating effective plastic strain

Using Eq. (24), the plastic work, defined by $\boldsymbol{\sigma} : \dot{\boldsymbol{\varepsilon}}^p$, can be re-written as

$$\boldsymbol{\sigma}_U : \dot{\boldsymbol{\varepsilon}}^p_U = \boldsymbol{\sigma}_U : \dot{\lambda}_U \frac{\partial \boldsymbol{\Phi}_U}{\partial \boldsymbol{\sigma}_U} = 2\,\dot{\lambda}_U\,\boldsymbol{\sigma}_U : \mathbb{G}^{\sigma}_U : \boldsymbol{\sigma}_U. \tag{28}$$

If we introduce the equivalent stress $\overline{\sigma}_U$ and plastic strain $\overline{\varepsilon}^p_U$ with the following identity

$$\boldsymbol{\sigma}_U : \dot{\boldsymbol{\varepsilon}}^p_U = \overline{\sigma}_U\,\dot{\overline{\varepsilon}}^p_U, \tag{29}$$

where $\overline{\sigma}_U$ is the effective stress that we have chosen to be defined by

$$\overline{\sigma}_U = \sigma^{\mathrm{iso}}_{\mathrm{y}}\,\boldsymbol{\sigma}_U : \mathbb{G}^{\sigma}_U : \boldsymbol{\sigma}_U, \tag{30}$$

by using Eqs. (28), (29) and (30), we can obtain the rate of accumulated equivalent plastic strain as

$$\dot{\overline{\varepsilon}}^p_U = \frac{2\,\dot{\lambda}_U}{\sigma^{\mathrm{iso}}_{\mathrm{y}}}. \tag{31}$$

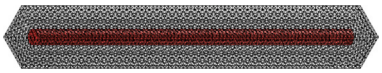

Fig. 3. FE mesh of the UC generated for the polyamide/glass SFRC with 10% of fiber volume fraction and fiber aspect ratio of 24. This UC is generated to obtain the unidirectional non-linear behavior of the composite.

5. Implementation

In this section, the implementation of the model, described in Sections 2–4, is explained in an incremental framework. The algorithmic steps include a first optional step of imposing uniaxial stress at the global configuration. In the second step, the strain state of each UC is obtained. Finally, the homogenized composite stress is calculated through orientation averaging of the individual UC stresses. In this section, we also provide some details on the surrogate model implementation.

5.1. Imposing uniaxial stress at the global configuration

In this study, a uniaxial stress framework is developed to predict the deformation behavior of SFRCs. The composite stress and strain tensors, using the Voigt notation, are given by

$$\boldsymbol{\sigma}_C = [\sigma_{C,11} \;\; \sigma_{C,22} \;\; \sigma_{C,33} \;\; \sigma_{C,12} \;\; \sigma_{C,13} \;\; \sigma_{C,23}]^{\mathrm{T}}, \tag{32}$$

$$\boldsymbol{\varepsilon}_C = [\varepsilon_{C,11} \;\; \varepsilon_{C,22} \;\; \varepsilon_{C,33} \;\; 2\varepsilon_{C,12} \;\; 2\varepsilon_{C,13} \;\; 2\varepsilon_{C,23}]^{\mathrm{T}}. \tag{33}$$

In this study, direction 11 is chosen to be the uniaxial stress direction. The composite stress and strain are represented by

$$\boldsymbol{\sigma}_C = \begin{bmatrix} \sigma_{C,\mathrm{I}} \\ \boldsymbol{\sigma}_{C,\mathrm{II}} \end{bmatrix}, \qquad \boldsymbol{\varepsilon}_C = \begin{bmatrix} \varepsilon_{C,\mathrm{I}} \\ \boldsymbol{\varepsilon}_{C,\mathrm{II}} \end{bmatrix}, \tag{34}$$

where $\varepsilon_{C,\mathrm{I}} = \varepsilon_{C,11}$ (imposed strain component); $\boldsymbol{\varepsilon}_{C,\mathrm{II}} = [\varepsilon_{C,22} \;\; \varepsilon_{C,33} \;\; 2\varepsilon_{C,12} \;\; 2\varepsilon_{C,13} \;\; 2\varepsilon_{C,23}]^{\mathrm{T}}$ (unconstrained strain components); $\sigma_{C,\mathrm{I}} = \sigma_{C,11}$ (uniaxial stress component); and $\boldsymbol{\sigma}_{C,\mathrm{II}} = [\sigma_{C,22} \;\; \sigma_{C,33} \;\; \sigma_{C,12} \;\; \sigma_{C,13} \;\; \sigma_{C,23}]^{\mathrm{T}}$ (null stress components). The relation between stress rate and strain rate is given by

$$\dot{\boldsymbol{\sigma}}_C = \mathbf{C}_C \;\; \dot{\boldsymbol{\varepsilon}}_C \tag{35}$$

where, $\mathbf{C}_C$ is the matrix representation of the elasto-plastic tangent stiffness of the composite. Then, in an incremental form, we have

$$\Delta\boldsymbol{\sigma}_C = \mathbf{C}_C \;\; \Delta\boldsymbol{\varepsilon}_C, \tag{36}$$

with $\Delta\boldsymbol{\sigma}_C = \boldsymbol{\sigma}_C^{n+1} - \boldsymbol{\sigma}_C^{n}$ and $\Delta\boldsymbol{\varepsilon}_C = \boldsymbol{\varepsilon}_C^{n+1} - \boldsymbol{\varepsilon}_C^{n}$ for a time increment $[t_n, t_{n+1}]$. In an incremental framework, using Forward-Euler approximation, we have:

$$\boldsymbol{\sigma}_C^{n+1} \approx \boldsymbol{\sigma}_C^{n} + \mathbf{C}_C^{n} \;\; \left[\boldsymbol{\varepsilon}_C^{n+1} - \boldsymbol{\varepsilon}_C^{n}\right]. \tag{37}$$

Eq. (37) can be re-written in matrix format as

$$\begin{bmatrix} \Delta\sigma_{C,\mathrm{I}} \\ \Delta\boldsymbol{\sigma}_{C,\mathrm{II}} \end{bmatrix} \approx \underbrace{\begin{bmatrix} \mathbf{C}_{C,(\mathrm{I,I})} & \mathbf{C}_{C,(\mathrm{I,II})} \\ \mathbf{C}_{C,(\mathrm{II,I})} & \mathbf{C}_{C,(\mathrm{II,II})} \end{bmatrix}^{n}}_{\mathbf{C}_C} \begin{bmatrix} \Delta\varepsilon_{C,\mathrm{I}} \\ \Delta\boldsymbol{\varepsilon}_{C,\mathrm{II}} \end{bmatrix}. \tag{38}$$

where,

$$\Delta\boldsymbol{\sigma}_{\mathrm{C}} = \boldsymbol{\sigma}_{\mathrm{C}}^{n+1} - \boldsymbol{\sigma}_{\mathrm{C}}^{n} \quad , \quad \Delta\boldsymbol{\varepsilon}_{\mathrm{C}} = \boldsymbol{\varepsilon}_{\mathrm{C}}^{n+1} - \boldsymbol{\varepsilon}_{\mathrm{C}}^{n}. \tag{39}$$

Using Eq. (38), the "II" component of the incremental stress is obtained as

$$\Delta\boldsymbol{\sigma}_{C,\mathrm{II}} \approx \mathbf{C}^{n}_{C,(\mathrm{II,I})} \;\Delta\varepsilon_{C,\mathrm{I}} + \mathbf{C}^{n}_{C,(\mathrm{II,II})} \;\Delta\boldsymbol{\varepsilon}_{C,\mathrm{II}}. \tag{40}$$

Obviously, to obtain an accurate approximation, it is required to have small load increments. The "II" component of the stress tensor at time step t_{n+1} ($\boldsymbol{\sigma}_{C,\mathrm{II}}^{n+1}$) has to be zero (to fulfill the uniaxial stress condition). Thus, using relations (39) and (40) and straightforward algebraic manipulations, the "II" component of the incremental strain is obtained as

$$\Delta\boldsymbol{\varepsilon}_{C,\mathrm{II}} \approx \left[\mathbf{C}^{n}_{C,(\mathrm{II,II})}\right]^{-1} \;\left[-\boldsymbol{\sigma}^{n}_{C,II} - \mathbf{C}^{n}_{C,(\mathrm{II,I})} \;\Delta\varepsilon_{C,\mathrm{I}}\right]. \tag{41}$$

Thus, the whole macroscopic (composite) strain is known ($\Delta\varepsilon_{C,\mathrm{I}}$ imposed, and $\Delta\boldsymbol{\varepsilon}_{C,\mathrm{II}}$ calculated). So far, the macroscopic (composite) strain state is obtained in an *approximate* approach for a *uniaxial stress state*.

5.2. Obtaining the strain state of each UC

Once the macroscopic incremental strain is known, the incremental strain of each UC is computed considering its orientation, and based on the interaction assumption.

5.2.1. Voigt assumption

For the Voigt assumption, the incremental UC strain is equal to the composite incremental strain ($\Delta\boldsymbol{\varepsilon}_U = \Delta\boldsymbol{\varepsilon}_C$). Thus, local incremental strain components of each UC are obtained by

$$\Delta\boldsymbol{\varepsilon}^{L}_{U,i} = \left[\mathbf{Q}(\mathbf{p}_i)\right] \;\Delta\boldsymbol{\varepsilon}_C, \tag{42}$$

where $\left[\mathbf{Q}(\mathbf{p}_i)\right]$ represents the matrix format of the fourth order tensor $\left[\mathbf{R}(\mathbf{p}_i) \,\overline{\otimes}\, \mathbf{R}(\mathbf{p}_i)\right]$. The subscript $_i$ represents the index of UCs which varies from 1 to the number of UCs in an aggregate.

5.2.2. Reuss assumption

With the Reuss assumption, it is assumed that the stress of each UC at the global configuration is equivalent to the composite stress ($\Delta\boldsymbol{\sigma}_U = \Delta\boldsymbol{\sigma}_C$). Thus, to have the incremental stress for each UC, we need to have the incremental stress for the composite which, using Forward-Euler approximation, is given by

$$\Delta\boldsymbol{\sigma}_C \approx \mathbf{C}^{n}_{C} : \Delta\boldsymbol{\varepsilon}_C. \tag{43}$$

Where the composite tangent stiffness from the previous time step ($\mathbf{C}^{n}_{C}$) is used. Now, we have an approximation of the incremental stress for each UC:

$$\Delta\boldsymbol{\sigma}_{U,i} = \Delta\boldsymbol{\sigma}_C. \tag{44}$$

This should be rotated to the local configuration to obtain the local stress state of each UC:

$$\Delta\boldsymbol{\sigma}^{L}_{U,i} = \left[\mathbf{Q}(\mathbf{p}_i)\right] \;\Delta\boldsymbol{\sigma}_{U,i}. \tag{45}$$

Using this approximated local incremental stress together with the tangent stiffness of each UC$_i$ from the previous increment, the incremental strain (approximated) of each UC is obtained:

$$\Delta\boldsymbol{\varepsilon}^{L}_{U,i} \approx (\mathbf{C}^{L,n}_{U,i})^{-1} \;\Delta\boldsymbol{\sigma}^{L}_{U,i}. \tag{46}$$

5.2.3. Self-consistent assumption

The incremental UC strain, considering the self consistent assumption, is given by

$$\Delta\boldsymbol{\varepsilon}_{U,i} = \left[\mathbf{I} + \mathbf{E}^{n+1}_{i} \;\left(\left[\mathbf{C}^{n+1}_{C}\right]^{-1} \;\mathbf{C}^{n+1}_{U,i} - \mathbf{I}\right)\right]^{-1} \;\Delta\boldsymbol{\varepsilon}_C. \tag{47}$$

Since the tangent stiffness of the UCs for time step t_{n+1} are not yet known, the corresponding stiffness at time step t_n ($\mathbb{C}^{n}_{U,i}$) is used instead.

$$\Delta\boldsymbol{\varepsilon}_{U,i} \approx \left[\mathbf{I} + \mathbf{E}^{n+1}_{i} \;\left(\left[\mathbf{C}^{n+1}_{C}\right]^{-1} \;\mathbf{C}^{n}_{U,i} - \mathbf{I}\right)\right]^{-1} \;\Delta\boldsymbol{\varepsilon}_C. \tag{48}$$

As explained before, the composite stiffness is obtained through a fixed point iterative procedure (using Eq. (48)). For the first iteration, the composite stiffness from the previous increment is considered. Now, the UC incremental strain should be rotated to the local configuration:

$$\Delta\boldsymbol{\varepsilon}^{L}_{U,i} = \left[\mathbf{Q}(\mathbf{p}_i)\right] \;\Delta\boldsymbol{\varepsilon}_{U,i}. \tag{49}$$

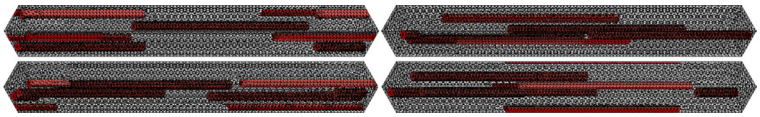

Fig. 4. FE mesh of the first series of unidirectional samples for the polyamide/glass SFRC: RVE length equal to 2 times fiber length, RVE width and thickness equal to 4 times fiber diameter, and fiber volume fraction of 10% and fiber aspect ratio of 24. These unidirectional samples are generated to evaluate the validity of the UC non-linear response.

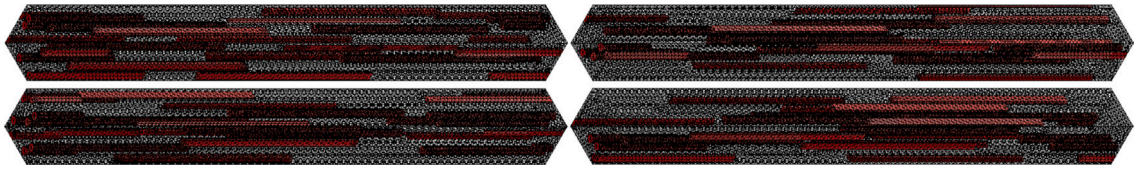

Fig. 5. FE mesh of the second series of unidirectional samples for the polyamide/glass SFRC: RVE length equal to 3 times fiber length, RVE width and thickness equal to 6 times fiber diameter, and fiber volume fraction of 10% and fiber aspect ratio of 24. These unidirectional composite samples are generated and analyzed for comparison purposes to confirm the validity of the proposed UC structure.

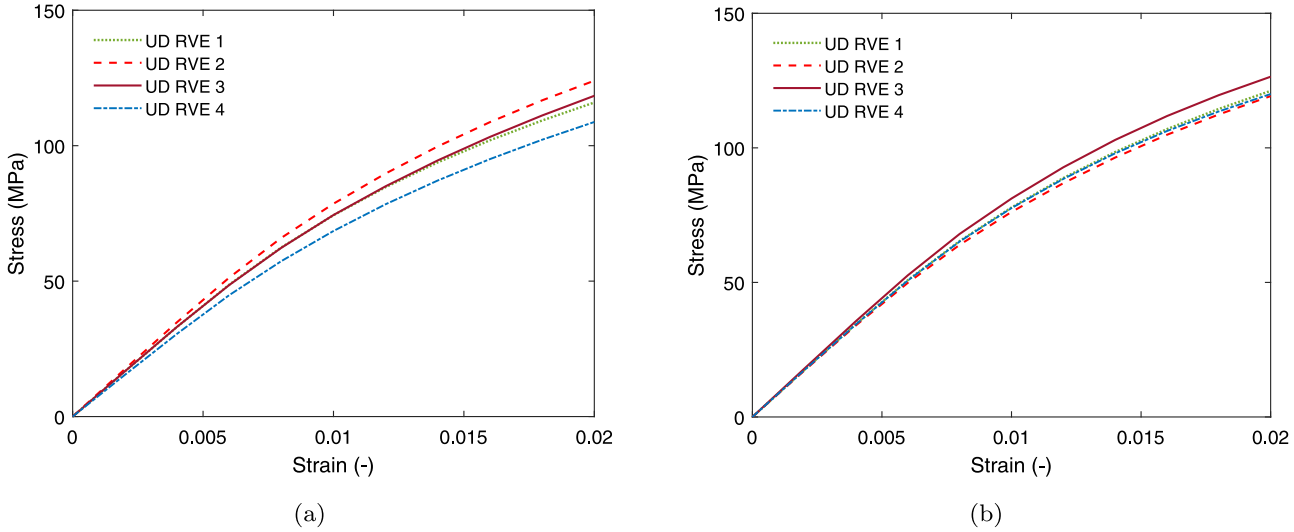

Fig. 6. Non-linear elasto-plastic stress–strain curves of UD RVEs of the polyamide/glass SFRC with fiber volume fraction of 10% and fiber aspect ratio of 24, subjected to uniaxial stress loading condition, (a): first series of samples shown in Fig. 4, (b): second series of samples shown in Fig. 5.

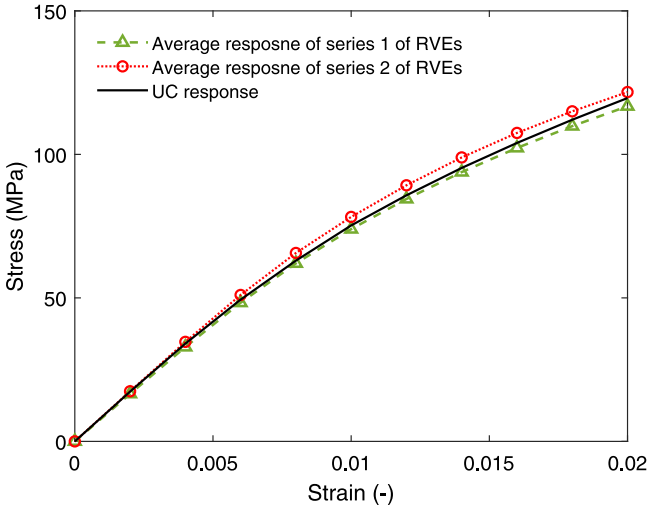

Fig. 7. Comparison of the average non-linear elasto-plastic stress–strain curves of UD RVEs and the UC of the polyamide/glass SFRC with fiber volume fraction of 10% and fiber aspect ratio of 24, subjected to uniaxial stress loading condition. Dashed line with triangle symbols: average response of series 1 of RVEs shown in Fig. 4; Dotted line with circle symbols: average response of series 2 of RVEs shown in Fig. 5.

5.3. Computing the homogenized (composite) stress

An incremental strain ($\Delta\boldsymbol{\varepsilon}^{L}_{U,i}$) is given for each of the UCs. The elastic trial stress at time t_{n+1} is obtained by

$$\boldsymbol{\sigma}^{L,n+1}_{U,i} = \boldsymbol{\sigma}^{L,n}_{U,i} + \mathbf{C}^{e}_{U}\,\Delta\boldsymbol{\varepsilon}^{L}_{U,i}. \tag{50}$$

Then, the yield function (Eq. (20)) is evaluated. If $\Phi_U < 0$ then, stress at t_{n+1} is the calculated trial stress (Eq. (50)) and $\bar{\varepsilon}^{p,n+1}_{U} = \bar{\varepsilon}^{p,n}_{U}$. On the other hand, if $\Phi_U \geq 0$, then we solve Eqs. (23) and (24) together with $\Phi_U = 0$ as

$$\mathbf{R} = \begin{bmatrix} \mathbf{R}_{\sigma} \\ \Phi_U \end{bmatrix} = \begin{bmatrix} \boldsymbol{\sigma}_U - \boldsymbol{\sigma}^{n}_{U} - \mathbf{C}^{e}_{U}\left(\Delta\boldsymbol{\varepsilon}^{L}_{U,i} - 2\,\Delta\lambda_U \mathbf{G}^{\sigma}_{U}\,\boldsymbol{\sigma}_U\right) \\ \boldsymbol{\sigma}_U\;\mathbf{G}^{\sigma}_{U}\;\boldsymbol{\sigma}_U - \alpha\left(\bar{\varepsilon}^{p}_{U}\right) \end{bmatrix}, \quad \mathbf{X} = \begin{bmatrix} \boldsymbol{\sigma}_U \\ \Delta\lambda_U \end{bmatrix}, \tag{51}$$

where $\Delta\lambda_U = \lambda^{n+1}_{U} - \lambda^{n}_{U}$ and $\bar{\varepsilon}^{p}_{U} = \bar{\varepsilon}^{p,n}_{U} + 2\,\Delta\lambda_U/\sigma^{\mathrm{iso}}_{\mathrm{y}}$. This equation system is solved using the Newton–Raphson procedure in standard fashion. Once the stresses of all the UCs are calculated, they are rotated back to the global configuration:

$$\boldsymbol{\sigma}^{n+1}_{U,i} = \left[\mathbf{Q}^{T}(\mathbf{p}_i)\right]\;\boldsymbol{\sigma}^{L,n+1}_{U,i}, \tag{52}$$

where $\left[\mathbf{Q}^{T}(\mathbf{p}_i)\right]$ is the matrix representation of fourth order tensor $\left[\mathbf{R}^{T}(\mathbf{p}_i) \otimes \mathbf{R}^{T}(\mathbf{p}_i)\right]$. The composite homogenized stress is obtained by

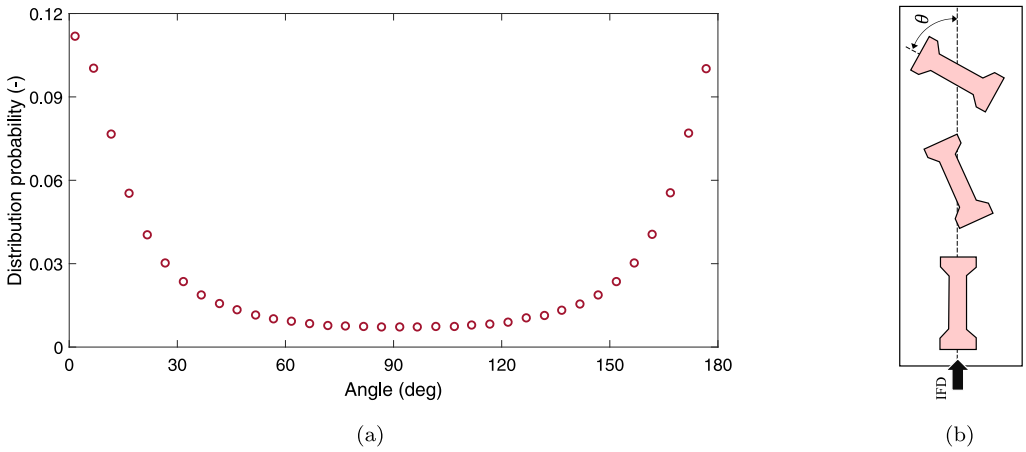

Fig. 8. (a): Planar and preferentially oriented distribution of fibers of the polyamide/glass SFRC reproduced after [37]. The preferential planar orientation gives rise to an anisotropic response, (b): Schematic representation of samples cut form an injection molded plate with different angles with respect to the Injection Flow Direction (IFD) in order to observe the anisotropic behavior resulted from the preferential fiber orientation distribution.

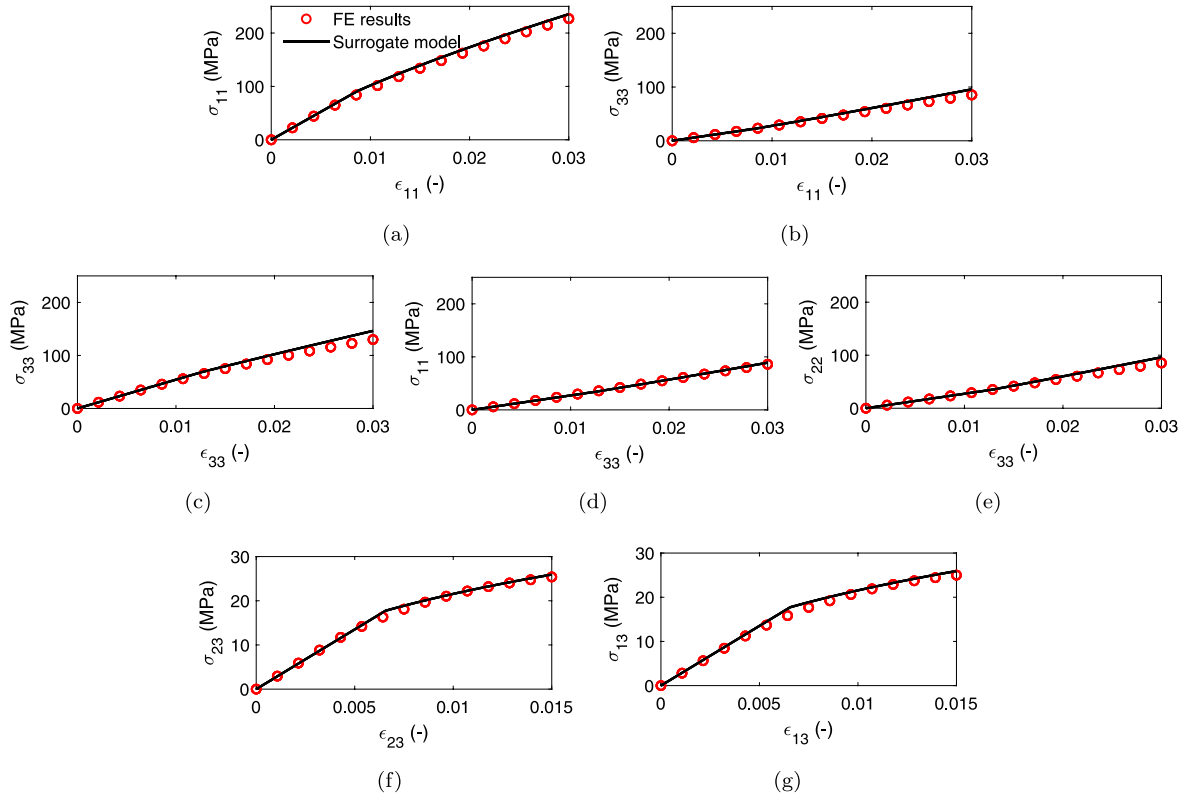

Fig. 9. Unit Cell finite element results (symbols) and predictions of the surrogate model (solid line) using the calibrated material properties for the polyamide/glass composite with fiber volume fraction of 10%, under different loading conditions: (a),(b): uniaxial strain in the longitudinal direction; (c),(d),(e): uniaxial strain in the transverse direction; (f),(g): shear loads.

$$\boldsymbol{\sigma}_C^{n+1} = \frac{1}{N_f} \sum_{i=1}^{N_f} \boldsymbol{\sigma}_{U,i}^{n+1}. \tag{53}$$

6. Results and discussion

In this paper, non-linear elasto-plastic stress–strain curves are obtained for two different SFRCs using the proposed model. Micro-structural characteristics of these composites are given in Table 1. For each of the SFRCs, initially, FE simulations are conducted on UCs, and then the surrogate model is calibrated using the UC Finite Element results.

Table 1
Micro-structural characteristics of SFRCs analyzed in this study.

Matrix	Polyamide	Polypropylene
Fibers	Glass	Flax
Fiber volume fraction	10%	13%
Fiber aspect ratio	24	75
Fiber length	240 μm	1200 μm
Fiber diameter	10 μm	16 μm
Orientation distribution	Preferential planar/3D random	3D random

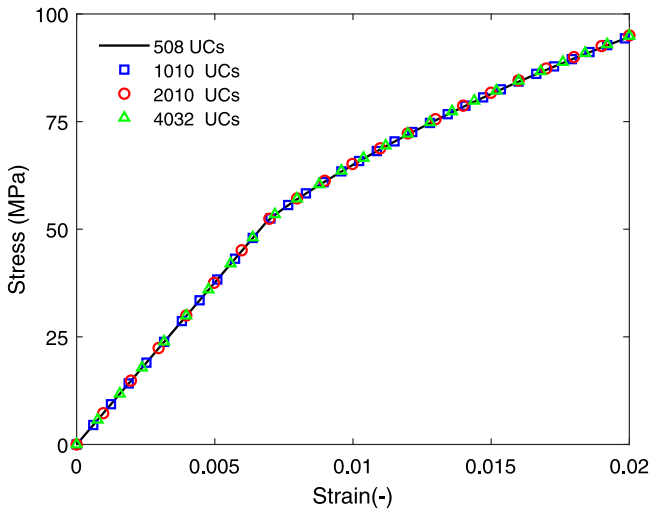

Fig. 10. Comparison of the non-linear elasto-plastic stress–strain curves obtained using the orientation averaging method and considering different number of UCs for the polyamide/glass SFRC at $\theta = 0°$ and using the Voigt interaction. It is obviously seen that the predictions of the orientation averaging method have no considerable dependency on the number of UCs for this SFRC.

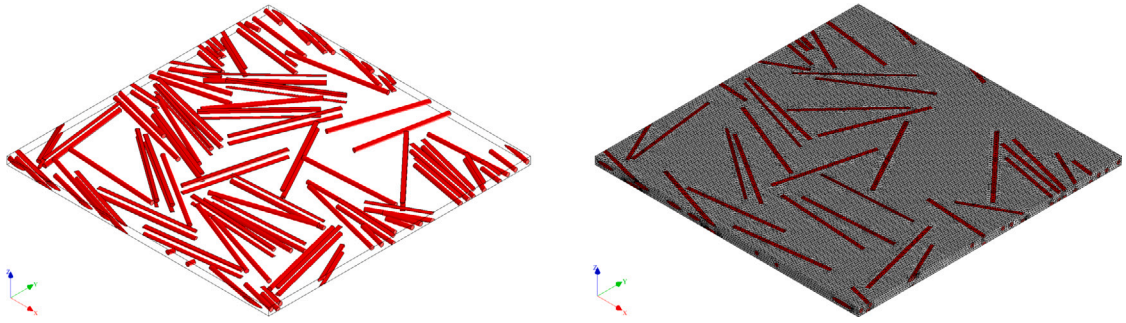

Fig. 11. The geometry of the analyzed micro-structural sample (for the polyamide/glass SFRC) and its spatial discretization. The length and width of the sample is equal to 720 μm which is three times the fiber length. The thickness of the sample is 20 μm which is two times the fiber diameter. The mesh includes 627,904 finite elements.

For calibrating the material properties of the surrogate model, an optimization algorithm is developed using Matlab optimization toolbox. The calibration process is performed in two steps: first, using the initial parts of FE stress–strain curves, the elastic properties are calibrated, and then, using the rest of the stress–strain curves, the yield and hardening parameters are optimized (while keeping the elastic properties unchanged).

Once the material properties are obtained, the proposed model is used to obtain the composite stress–strain curves. Before modeling of the SFRCs, an evaluation of the UC structure and its validity for the proposed model is performed.

6.1. Investigating the UC validity

Regarding the geometrical aspects of the UC, the same distance is considered from the fiber to all sides of the UC. Then, considering the fiber dimensions and with respect to fiber volume fraction, the UC dimensions are obtained. To check the validity of the proposed UC structure, analyses are performed on unidirectional samples and the results are compared to the UC response. Two different set of UD RVEs are generated and analyzed for a polyamide/glass SFRC studied by Kammoun et al. [37]. In the first set, the RVE length was set 2 times the fiber length, and the RVE width and thickness to 4 times fiber diameter. In the second set, the RVE length was chosen as 3 times the fiber length, and the RVE width and thickness as 6 times the fiber diameter. Fiber Volume fraction of 10% is considered. The FE mesh of the analyzed UC and two RVE sets are shown in Figs. 3–5.

The RVE generations and analyses are performed using Digimat-FE [42], and under periodic boundary conditions. Uniaxial stress loading in the fiber directions is imposed. The obtained stress–strain curves are shown in Fig. 6. A comparison between the UC response and the average response of the unidirectional samples is shown in Fig. 7. A good correlation is seen between the response of the UC and unidirectional samples, and thus, it is reasonable to use the UC response within the OA modeling approach for the studied SFRC.

Remark 1. For the analyzed case, the proposed UC structure has shown to be a good representative for the unidirectional behavior (see Fig. 7). Nevertheless, it is advisable to analyze a UD RVE for a generic SFRC with arbitrary matrix and fiber constitutive properties and fiber geometries, to make sure about the representativeness of the obtained results

6.2. A polyamide/glass SFRC

Elasto-plastic response of an SFRC made from Polyamide 6.6 (PA 6.6) matrix reinforced with $V_f = 10\%$ of short glass fibers is obtained. The fiber length and diameter are $l_f = 240$ μm and $d_f = 10$ μm which result in an aspect ratio of $\lambda = 24$. Fibers have a planar distribution with a preferred direction which is caused by the injection molding fabrication process. Fig. 8(a) shows the preferentially planar orientation distribution of fibers in the composite. Kammoun et al. [37] cut samples from the injection molded plate with different angles with respect to the Injection Flow Direction (IFD). This is schematically shown in Fig. 8(b).

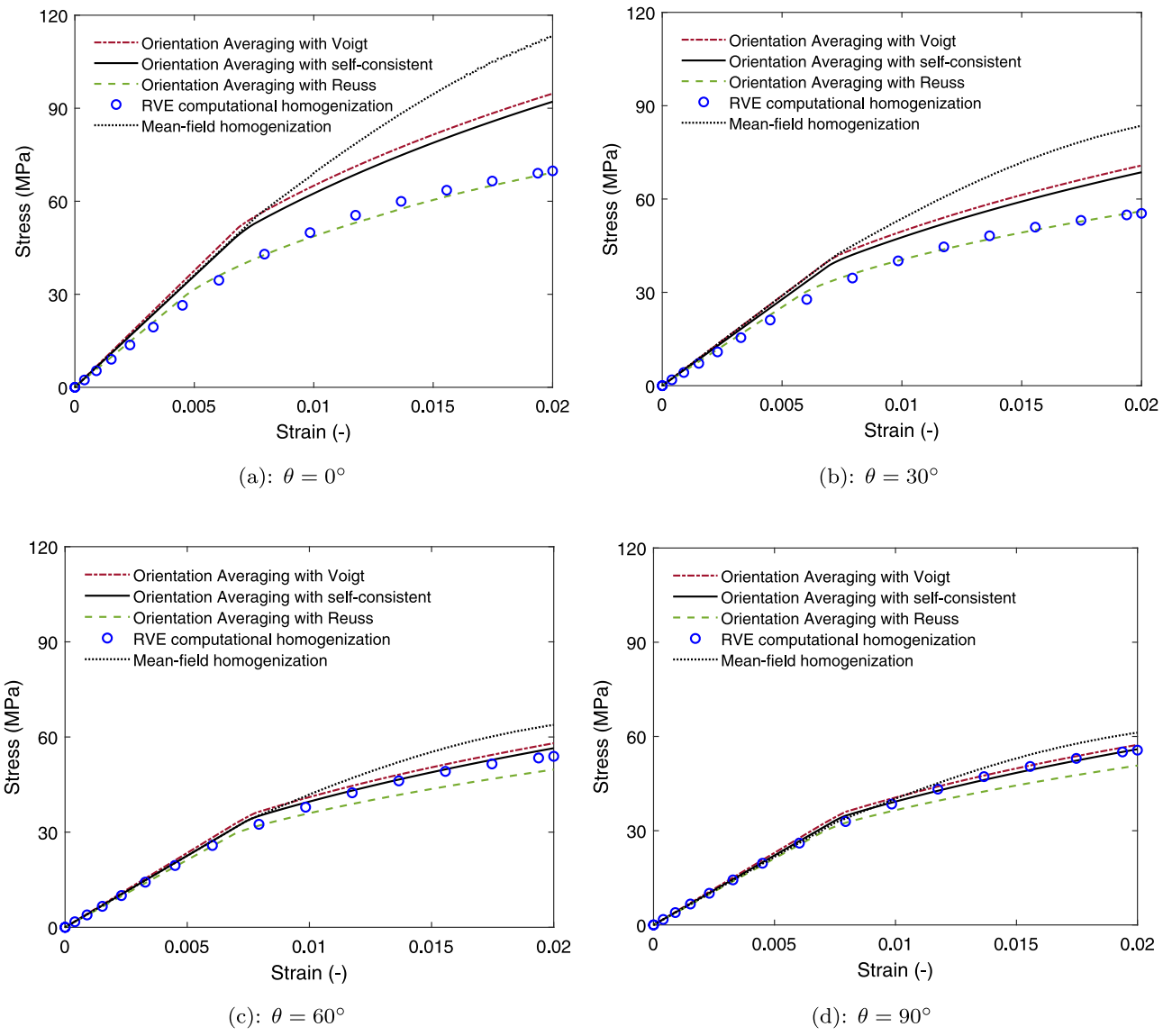

Fig. 12. Comparison of the non-linear elasto-plastic stress–strain curves of the polyamide/glass SFRC, with fiber volume fraction of 10%, obtained using the orientation averaging method, RVE finite element simulations, and mean-field homogenization. Different cutting angles ($\theta = 0°, 30°, 60°, 90°$) with respect to the injection flow direction is considered. This means that for each angle (other than $\theta = 0°$) the orientation distribution has been rotated by the corresponding angle. The anisotropic behavior due to the preferential orientation distribution is observed in the stress–strain curves at different angles.

Table 2
Constitutive properties of the matrix and reinforcements of the polypropylene/flax SFRC.

Parameter	Fibers		Matrix					
	E_f (GPa)	ν_f (-)	E_m (GPa)	ν_m (-)	σ_y (MPa)	k (MPa)	R_∞ (MPa)	m (-)
Value	76	0.22	3.1	0.35	25	150	20	325

Glass fibers are elastic, and the matrix material obeys J_2 plasticity, with isotropic linear–exponential hardening:

$$R(\bar{\varepsilon}^p) = k\bar{\varepsilon}^p + R_\infty \left[1 - \exp(-m\bar{\varepsilon}^p)\right], \tag{54}$$

where $\bar{\varepsilon}^p$ is accumulated plastic strain, K, R_∞ and m are material parameters. The yield stress if the matrix is not provided (as confidential data) by the reference authors [37]. Also, the hardening parameters are given as functions of the yield stress value: $k = 6\sigma_y$ and $R_\infty = 0.8\sigma_y$. We assumed a yield stress of $\sigma_y = 25$ MPa for the matrix, and obtained the hardening parameters accordingly. The constitutive properties for both constituents are summarized in Table 2. To obtain the UC behavior, four loading cases are applied: unaxial strain in the fiber direction, uniaxial strain in the transverse direction, and two shear cases. Then, the optimization algorithm is used, together with the surrogate model, to obtain the UC constitutive properties. The UC Finite Element results together with the predictions of the surrogate model (with calibrated properties) are shown in Fig. 9. The UC fitted material properties (for the surrogate model) are given in Table 3.

To conduct the OA simulations, it is required to know how many UCs are needed to have a representative aggregate. To do so, simulations are conducted with different number of UCs, namely 508, 1010, 2010 and 4032 (for $\theta = 0°$, and with Voigt assumption). The obtained results are shown in Fig. 10. No noticeable dependency on the number of UCs is observed for this composite.

Simulations are conducted for four different angles, namely $\theta = 0°, 30°, 60°$ and $90°$ (specimen cut angles with respect to the injection

Table 3
Quantified material properties for the polyamide/glass composite.

Parameter	E (GPa)	ν (−)	C (−)	σ_{y0} (MPa)	R_σ (−)	H_1 (−)	H_2 (−)	H_3 (−)
Value	3.856	0.335	1.937	33.032	6.525	493.521	14.996	10.067

Table 4
Constitutive properties of the matrix and reinforcements of the polypropylene/flax SFRC [44].

Parameter	Fibers		Matrix				
	E_f (GPa)	ν_f (-)	E_m (GPa)	ν_m (-)	σ_0 (MPa)	a (-)	n (-)
Value	69	0.15	1.6	0.4	16	0.235	5.44

flow direction). Also, Finite Element simulations were conducted on a micro-structural sample using Digimat-FE. The geometry of the sample and its spatial discretization are shown in Fig. 11. To generate the micro-structural sample, first, the fiber orientation tensor was calculated from the orientation distribution function. The obtained second order orientation tensor was then used for creating a sample. The length and width of the micro-structural sample was set to 3 times the fiber length (720 μm), and the thickness to 2 times the fiber diameter (20 μm). A number of samples were generated to obtain one which had an acceptable fiber orientation distribution. The sample was spatially discretized with 627904 finite elements, and periodic boundary conditions were imposed on the boundaries. Also, mean-field Mori–Tanaka simulations were conducted using Digimat-MF for comparison purposes. The obtained stress–strain curves using the OA method (all interactions), RVE computational homogenization, and mean-field homogenization are shown in Fig. 12. It is seen that the effect of orientation distribution and interaction assumption is captured in the OA simulations. Also, similar trends as in the RVE results are observed in the OA simulations. In comparison to mean-field results, the predictions of the OA method have a better agreement with the RVE simulations. However, using these results, drawing solid conclusions regarding the interactions and their suitability is not possible, due to the followings:

(I) The orientation distribution tensor from the micro-structural sample was not exactly the input (desired) orientation tensor (obtained from orientation distribution function), but still the best achieved by the authors;

(II) No statistical analyses were performed to obtain the RVE size (see e.g. [43]). This was not only because reaching desired orientation distribution was found to be very difficult, but also because simulating bigger samples (than the analyzed one) was found to be very challenging (with the used package).

6.3. A Polypropylene/flax SFRC

In this section, an SFRC, made from a polypropylene reinforced with 13% (volume fraction) of short flax fibers, is modeled. Fibers have a length of $l_f = 1200$ μm, and a diameter of $d_f = 16$ μm which lead to an aspect ratio of $\lambda = 75$, and they are randomly distributed. The matrix is modeled as an elasto-plastic material using the Ramberg–Osgood model, and the fibers are considered elastic. In a uniaxial loading condition, stress and strain are related by [44]:

$$\varepsilon = \frac{\sigma}{E}\left(1 + a\left(\frac{\sigma}{\sigma_0}\right)^{n-1}\right), \tag{55}$$

where, E is the Young's modulus and a, σ_0 and n are the model parameters.Table 4 gives the material properties for the matrix and reinforcements [44].

Similarly to the SFRC in the previous section, the UC was subjected to four loading cases, and FE results were obtained under periodic boundary conditions. The FE results were used to calibrate the material parameters for the surrogate model, given in Table 5.

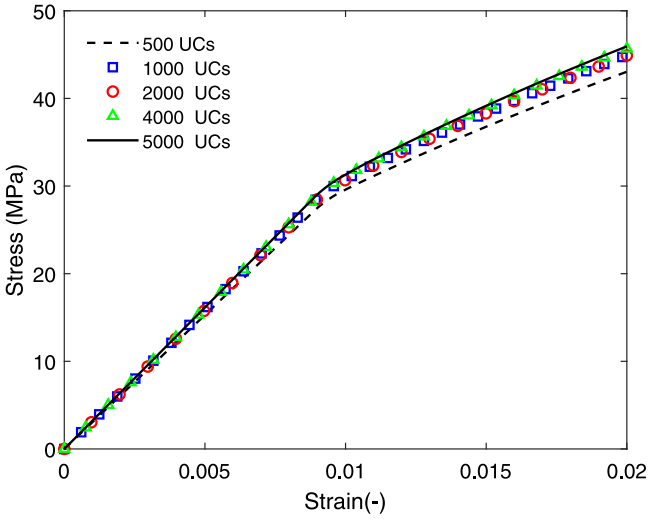

Fig. 13. Comparison of the non-linear elasto-plastic stress–strain curves obtained using the orientation averaging method and considering different number of UCs for the Polypropylene/flax SFRC with 13% of fiber volume fraction, and using the Voigt interaction. Based on this comparison, 5000 UCs is considered as a representative number for the OA simulations of this bio-composite.

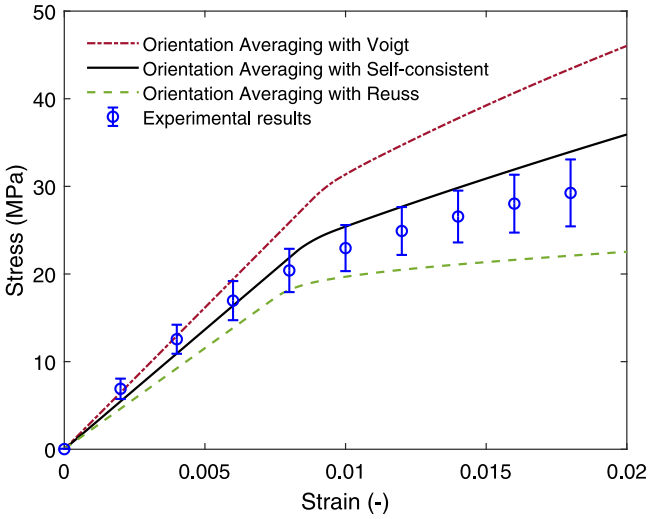

Fig. 14. Non-linear elasto–plastic stress–strain curves obtained for the polypropylene/flax bio-composite with 13% of fiber volume fraction using the orientation averaging method and different interactions, namely Voigt, Reuss and self-consistent assumptions, together with experimental results taken from [44].

In order to find out the number of required UCs for the analysis of this SFRC, a sensitivity analysis is performed. The stress–strain curves obtained using the Voigt interaction is shown in Fig. 13. It is found out that 5000 UCs is a representative number for simulations of this composite.

The obtained results using the developed model are compared to experimental results, taken from [44]. The experimental results are shown by the average of the stress–strain curves with error bars representing the bounds of standard deviation. It is seen in Fig. 14 that the model provides a reasonable prediction of the stress–strain curve, particularly with the self-consistent interaction.

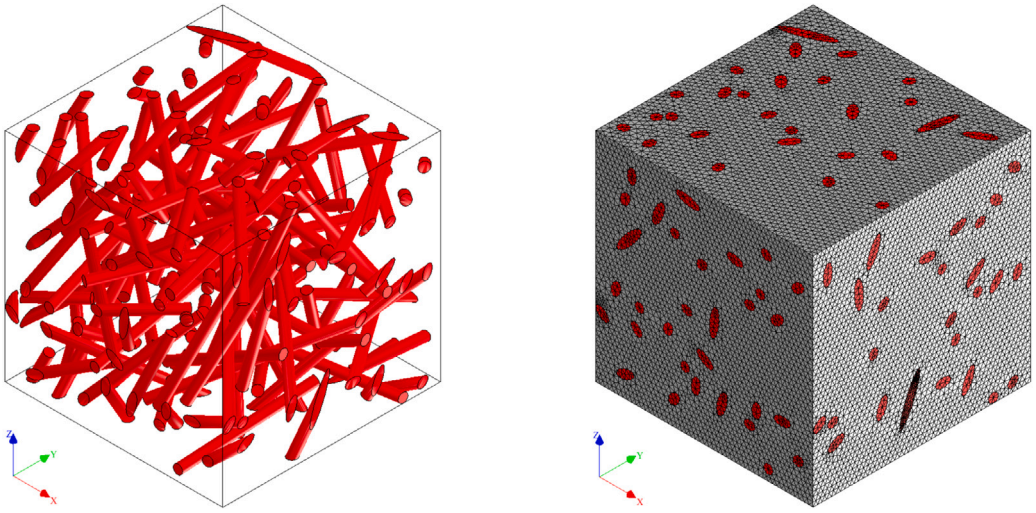

Fig. 15. The geometry of the analyzed micro-structural sample (for the virtual random 3D polyamide/glass SFRC) and its spatial discretization. The dimensions of the microstructural sample are considered equivalent to the fiber length (240 μm × 240 μm × 240 μm). The mesh includes 664,816 finite elements.

Table 5
Quantified material properties for the polypropylene/flax composite.

Parameter	E (GPa)	ν (−)	C (−)	σ_{y0} (MPa)	R_σ (−)	H_1 (−)	H_2 (−)	H_3 (−)
Value	1.989	0.389	2.769	19.984	47.739	131.161	11.965	10.036

Remark 2. It is well-understood that the properties of a composite material is affected by the matrix–fiber interfacial properties (see e.g. [45,46]). Different approaches are used for modeling the interface properties. For a review of different analytical models to study fiber pull-out behavior to characterize matrix–fiber adhesion, an interested reader is referred to [47]. The classical shear lag theory, proposed by Cox [48], has been widely used for modeling interface debonding in composite materials (see e.g. [49–51]). In this study, we considered a perfect bonding between the matrix and fibers. In principal, it is possible to consider matrix–fiber debonding using a cohesive zone interface in the FE simulations. However, it is then most probably required to extend the surrogate model (described in Section 4) so that this damage mechanism is properly captured by the model. Thus, for SFRCs with rather weak interface properties, such as natural fiber composites (see e.g. [52,53]), the current model should be used with care.

From Fig. 14, it is seen that in the non-linear regime, even the self-consistent interaction slightly overestimates the experimental results. This suggests that the assumption of matrix–fiber *perfect* bonding is probably not completely realistic.

A few efforts were also given to perform computational homogenization on realistic RVEs, and compare the results to the OA model predictions. The authors did not manage to generate RVEs, due to high aspect ratio of fibers and their random 3D distribution.

6.4. A virtual Polyamide/glass SFRC

To make a direct comparison of the computational efficiency of the model with computational homogenization, a virtual material is generated using the constituents and their mechanical properties (polyamide and glass) of the SFRC described in Section 6.2. A random 3D fiber orientation distribution is considered.

The geometry of the analyzed microstructural sample (in the case of computational homogenization) and its spatial discretization are shown in Fig. 15. The dimensions of the microstructural sample are 240 μm × 240 μm × 240 μm which is equivalent to the fiber length. The sample is spatially discretized with 664,816 finite elements, and periodic boundary conditions are considered.[3] A uniaxial stress state is imposed with a macroscopic strain of 3%, and the simulation took 17,684 s.

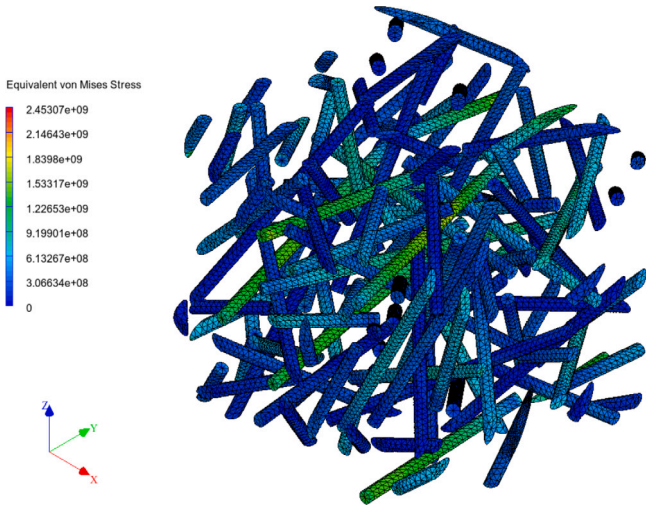

Fig. 16. Contour plot of the equivalent von Mises stress in the fibers of the virtual random 3D polyamide/glass SFRC subjected to uniaxial stress loading condition. Only fibers are shown in the contour plot since the load in mainly carried by the fibers.

The contour plot of equivalent von Mises stress in the fibers is shown in Fig. 16.

For the orientation averaging simulations, first, a sensitivity analysis is conducted to make sure about the required number of UCs. Simulations are performed using 500, 1000, 2000, and 4000 UCs and using the self-consistent interaction. Fig. 17 shows the obtained stress–strain curves where no considerable dependency on the number of UCs

[3] The authors tried to analyze bigger samples as well, but no successful execution of the problem is achieved with the used package and a personal computer.

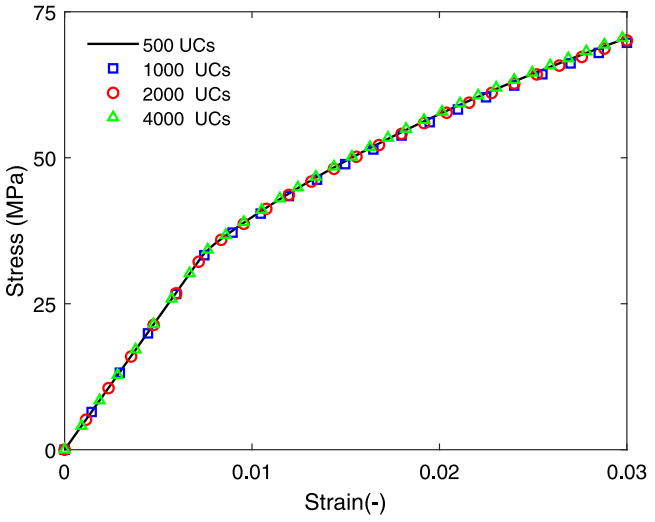

Fig. 17. Comparison of the non-linear elasto-plastic stress–strain curves obtained for the virtual polyamide/glass SFRC using the orientation averaging method with the self-consistent interaction, and considering different number of UCs. It is seen that the OA method has no considerable dependency on the number of UCs for this SFRC.

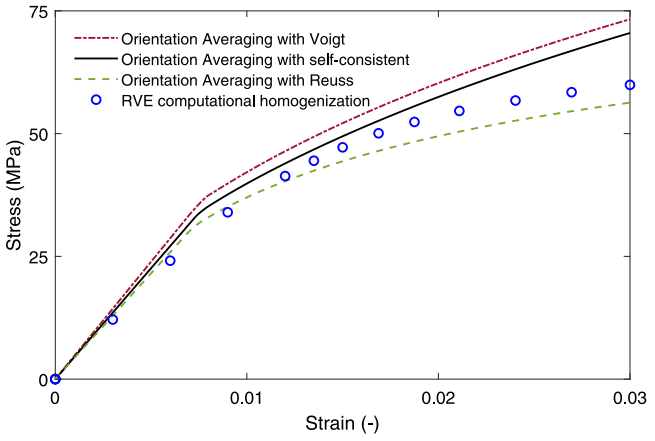

Fig. 18. Non-linear elasto-plastic stress–strain curves obtained for the virtual polyamide/glass SFRC using the orientation averaging method and different interactions, namely Voigt, Reuss and self-consistent assumptions, together with the results obtained from RVE computational homogenization simulations.

can be observed for this material. Thus, 500 UCs is considered as a representative number for the OA simulations of this material.

The predictions from the orientation averaging based homogenization, for all three interactions, together with RVE computational homogenization results, are shown in Fig. 18. As mentioned before, analysis of bigger RVEs (in computational homogenization) proved to be challenging, and thus, the analyzed microstructural sample may not be fully representative for the material (see [54–56]). Hence, it is difficult to draw an absolute conclusion from the comparison (orientation averaging vs RVE computational homogenization) in Fig. 18. Nevertheless, it can be observed that a reasonable agreement is obtained between the two approaches.

Furthermore, a very important aspect of the developed model is its computational efficiency. Fig. 19 shows a comparison of the calculation time using the two different methods. It is seen that the OA method is much faster than the computational homogenization method, even with the self-consistent interaction which is the most computationally expensive interaction (among the three interactions).

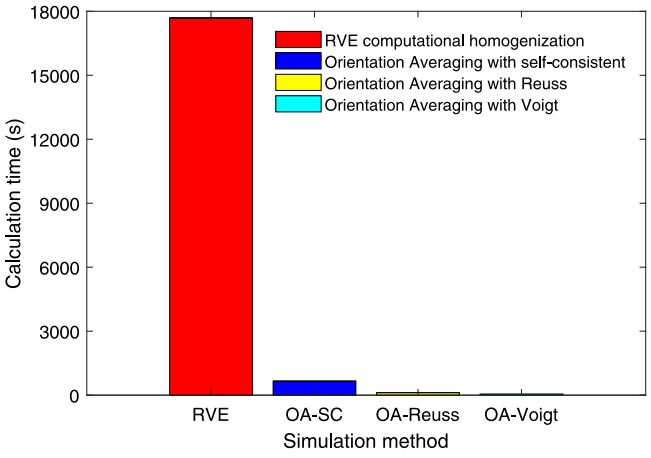

Fig. 19. Comparison of the calculation time of the analysis of the 3D random polyamide/glass SFRC using RVE computational homogenization and the orientation averaging method with self-consistent, Voigt and Reuss interactions. Remarkably faster simulations are achieved using the OA method in comparison with the RVE finite element simulations.

7. Conclusions

In this paper, a micro-mechanical model based on Orientation Averaging was developed to predict non-linear elasto-plastic behavior of Short Fiber Reinforced Composites. As a micromechanical basis for the model, the nonlinear mechanical response of a single elastic fiber surrounded by an elasto-plastic matrix was estimated through Finite Element Analyses performed on an idealized Unit Cell. To promote computational speed and flexibility of the model, the unit cell FEA results were then used to calibrate an elasto-plastic surrogate model to represent the single fiber–matrix behavior in the subsequent homogenization to macroscale behavior. For the homogenization to macroscale behavior, a novel incremental orientation averaging procedure, utilizing the tangent stiffness of the surrogate model, was proposed for which three alternative interactions were considered, namely Voigt, Reuss and self-consistent interactions.

A current limitation of the model is the assumption of perfect bonding between the matrix and the fibers. It is acknowledged that this restricts the application of the current version of the model to e.g., natural fiber composites undergoing large deformations, as these composites suffer from a rather weak fiber–matrix interface. Still, the authors believe that the modeling approach presented in this study has several advantages compared to other methods available in the literature.

First of all, the model is very relevant for computationally efficient modeling of short fiber reinforced composites produced via e.g., injection molding which possess a varying fiber orientation distribution in different sections of the final part. Compared to e.g., models based on computational homogenization, the proposed model has almost no limitation with respect to fiber aspect ratio, fiber volume fraction and fiber orientation distribution, among other properties. Thus, it does not suffer from the challenge of generating realistic RVEs based on actual material microstructures, as necessary for computational homogenization approach, which is not always straightforward. Neither does it require the same extent of heavy calculations of individual RVEs at different points.

Furthermore, using FEA at the UC level not only gives accurate predictions, but also provides the possibility to extend the model in order to include other micro-structural phenomena such as a varying fiber length distribution, and the occurrence of matrix–fiber debonding.

In terms of prediction capability, the effects of oriented fiber distributions (leading to an anisotropic behavior) were captured by the model, and adequate agreements were obtained when comparing the model predictions to both RVE analyses and experimental results.

CRediT authorship contribution statement

S.M. Mirkhalaf: Conceptualization, Methodology, Software, Validation, Formal analysis, Investigation, Data curation, Writing – original draft, Writing – review & editing, Visualization, Supervision, Project administration, Funding acquisition. **T.J.H. van Beurden:** Methodology, Software. **M. Ekh:** Software, Writing – original draft, Writing – review & editing. **F. Larsson:** Conceptualization, Methodology, Writing – review & editing, Supervision. **M. Fagerström:** Conceptualization, Methodology, Writing – review & editing, Supervision, Project administration, Funding acquisition.

Declaration of competing interest

The authors declare that they have no known competing financial interests or personal relationships that could have appeared to influence the work reported in this paper.

Acknowledgments

S.M. Mirkhalaf is thankful for the financial support from the Swedish Research Council (VR grant: 2019-04715) and the University of Gothenburg, Sweden. T.J.H. van Beurden acknowledges financial support from the Erasmus+ programme of the European Union. M. Fagerström gratefully acknowledges the support through Vinnova's strategic innovation programme LIGHTer and Area of Advance, Materials Science at Chalmers University of Technology, Sweden. The authors would also like to thank e-Xstream for providing a license of software Digimat.

References

[1] Kammoun S, Doghri I, Brassart L, Delannay L. Micromechanical modeling of the progressive failure in short glass–fiber reinforced thermoplastics – First Pseudo-Grain damage model. Composites Part A Appl Sci Manuf 2015;73:166–75. http://dx.doi.org/10.1016/j.compositesa.2015.02.017, URL http://www.sciencedirect.com/science/article/pii/S1359835X1500069X.

[2] Doghri I, Ouaar A. Homogenization of two-phase elasto-plastic composite materials and structures: Study of tangent operators, cyclic plasticity and numerical algorithms. Int J Solids Struct 2003;40(7):1681–712. http://dx.doi.org/10.1016/S0020-7683(03)00013-1, URL http://www.sciencedirect.com/science/article/pii/S0020768303000131.

[3] Doghri I, Brassart L, Adam L, Gérard JS. A second-moment incremental formulation for the mean-field homogenization of elasto-plastic composites. Int J Plast 2011;27(3):352–71. http://dx.doi.org/10.1016/j.ijplas.2010.06.004.

[4] Wu L, Doghri I, Noels L. An incremental-secant mean-field homogenization method with second statistical moments for elasto-plastic composite materials. Phil Mag 2015;95(28–30):3348–84. http://dx.doi.org/10.1080/14786435.2015.1087653.

[5] Wu L, Adam L, Doghri I, Noels L. An incremental-secant mean-field homogenization method with second statistical moments for elasto-visco-plastic composite materials. Mech Mater 2017;114:180–200. http://dx.doi.org/10.1016/j.mechmat.2017.08.006.

[6] Huang Zheng-Ming, Zhang Chun-Chun, Xue Yuan-De. Stiffness prediction of short fiber reinforced composites. Int J Mech Sci 2019;161–162:105068. http://dx.doi.org/10.1016/j.ijmecsci.2019.105068, URL https://www.sciencedirect.com/science/article/pii/S002074031932017X.

[7] Selmi A, Doghri I, Adam L. Micromechanical simulations of biaxial yield, hardening and plastic flow in short glass fiber reinforced polyamide. Int J Mech Sci 2011;53(9):696–706. http://dx.doi.org/10.1016/j.ijmecsci.2011.06.002, URL https://www.scopus.com/inward/record.uri?eid=2-s2.0-80051550439&doi=10.1016%2fj.ijmecsci.2011.06.002&partnerID=40&md5=22a2b4fd06989078a82a13b91ea7290a. cited By 16.

[8] Mirkhalaf M, van Dommelen JAW, Govaert LE, Furmanski J, Geers MGD. Micromechanical modeling of anisotropic behavior of oriented semicrystalline polymers. J Polym Sci Part B: Polym Phys 2019;57(7):378–91. http://dx.doi.org/10.1002/polb.24791, URL https://www.scopus.com/inward/record.uri?eid=2-s2.0-85061446380&doi=10.1002%2fpolb.24791&partnerID=40&md5=57d95ad08cec471aa9afc82a3124f70c. cited By 4.

[9] Heidari-Rarani M, Bashandeh-Khodaei-Naeini K, Mirkhalaf SM. Micromechanical modeling of the mechanical behavior of unidirectional composites – A comparative study. J Reinf Plast Compos 2018;37(16):1051–71, URL https://www.scopus.com/inward/record.uri?eid=2-s2.0-85047661544&doi=10.1177%2f0731684418779441&partnerID=40&md5=4c75382ab5584933e8451d6e0efb2e91.

[10] Eshelby JD. He determination of the elastic field of an ellipsoidal inclusion, and related problems. Proc R Soc Lond Ser A Math Phys Sci 1957;241(1226):376–96, URL http://micro.stanford.edu/~caiwei/me340b/content/me340b-notes_v01.pdf.

[11] Hashin Z, Shtrikman S. On some variational principles in anisotropic and nonhomogeneous elasticity. J Mech Phys Solids 1962;10(4):335–42. http://dx.doi.org/10.1016/0022-5096(62)90004-2, URL https://www.sciencedirect.com/science/article/pii/0022509662900042.

[12] Hashin Z, Shtrikman S. A variational approach to the theory of the elastic behaviour of multiphase materials. J Mech Phys Solids 1963;11(2):127–40. http://dx.doi.org/10.1016/0022-5096(63)90060-7, URL https://www.sciencedirect.com/science/article/pii/0022509663900607.

[13] Hill R. A self-consistent mechanics of composite materials. J Mech Phys Solids 1965;13(4):213–22. http://dx.doi.org/10.1016/0022-5096(65)90010-4, URL https://www.sciencedirect.com/science/article/pii/0022509665900104.

[14] Budiansky B. On the elastic moduli of some heterogeneous materials. J Mech Phys Solids 1965;13(4):223–7. http://dx.doi.org/10.1016/0022-5096(65)90011-6, URL https://www.sciencedirect.com/science/article/pii/0022509665900116.

[15] Mori T, Tanaka K. Average stress in matrix and average elastic energy of materials with misfitting inclusions. Acta Metall 1973;21(5):571–4. http://dx.doi.org/10.1016/0001-6160(73)90064-3, URL http://www.sciencedirect.com/science/article/pii/0001616073900643.

[16] Hessman Patrick Arthur, Welschinger Fabian, Hornberger Kurt, Böhlke Thomas. On mean field homogenization schemes for short fiber reinforced composites: Unified formulation, application and benchmark. Int J Solids Struct 2021;230–231:111141. http://dx.doi.org/10.1016/j.ijsolstr.2021.111141, URL https://www.sciencedirect.com/science/article/pii/S0020768321002316.

[17] Tian W, Qi L, Zhou J, Liang J, Ma Y. Representative volume element for composites reinforced by spatially randomly distributed discontinuous fibers and its applications. Compos Struct 2015;131:366–73. http://dx.doi.org/10.1016/j.compstruct.2015.05.014.

[18] Qi L, Tian W, Zhou J. Numerical evaluation of effective elastic properties of composites reinforced by spatially randomly distributed short fibers with certain aspect ratio. Compos Struct 2015;131:843–51.

[19] Tikarrouchine E, Chatzigeorgiou G, Praud F, Piotrowski B, Chemisky Y, Meraghni F. Three-dimensional FE2method for the simulation of non-linear, rate-dependent response of composite structures. Compos Struct 2018;193(March):165–79. http://dx.doi.org/10.1016/j.compstruct.2018.03.072.

[20] Mirkhalaf M, Ashrafi B. A numerical study on improving the specific properties of staggered composites by incorporating voids. Mater Today Commun 2017;13:144–54. http://dx.doi.org/10.1016/j.mtcomm.2017.09.011, URL http://www.sciencedirect.com/science/article/pii/S2352492817302210.

[21] Spahn J, Andrä H, Kabel M, Müller R. A multiscale approach for modeling progressive damage of composite materials using fast Fourier transforms. Comput Methods Appl Mech Eng 2014;268:871–83. http://dx.doi.org/10.1016/j.cma.2013.10.017, URL https://www.sciencedirect.com/science/article/pii/S0045782513002697.

[22] Schneider M, Ospald F, Kabel M. Computational homogenization of elasticity on a staggered grid. Int J Numer Methods Eng 2016;105(9):693–720. http://dx.doi.org/10.1002/nme.5008, URL https://www.scopus.com/inward/record.uri?eid=2-s2.0-84956592567&doi=10.1002%2fnme.5008&partnerID=40&md5=16db522cfcc01c880eaceda600136491. cited By 86.

[23] Pan Y, Iorga L, Pelegri AA. Numerical generation of a random chopped fiber composite RVE and its elastic properties. Compos Sci Technol 2008;68(13):2792–8. http://dx.doi.org/10.1016/j.compscitech.2008.06.007.

[24] Bargmann S, Klusemann B, Markmann J, Schnabel JE, Schneider K, Soyarslan C, Wilmers J. Generation of 3D representative volume elements for heterogeneous materials: A review. Prog Mater Sci 2018;96:322–84. http://dx.doi.org/10.1016/j.pmatsci.2018.02.003, URL http://www.sciencedirect.com/science/article/pii/S0079642518300161.

[25] Mirkhalaf SM, Eggels EH, Anantharanga AT, Larsson F, Fagerström M. Short fiber composites: Computational homogenization vs orientation averaging. ICCM22 2019 2019;3000.

[26] Gusev Andrei A. Representative volume element size for elastic composites: A numerical study. J Mech Phys Solids 1997;45(9):1449–59. http://dx.doi.org/10.1016/S0022-5096(97)00016-1, URL https://www.sciencedirect.com/science/article/pii/S0022509697000161.

[27] Böhm HJ, Eckschlager A, Han W. Multi-inclusion unit cell models for metal matrix composites with randomly oriented discontinuous reinforcements. Comput Mater Sci 2002;25(1):42–53. http://dx.doi.org/10.1016/S0927-0256(02)00248-3, URL https://www.sciencedirect.com/science/article/pii/S0927025602002483.

[28] Pan Yi, Iorga Lucian, Pelegri Assimina A. Analysis of 3D random chopped fiber reinforced composites using FEM and random sequential adsorption. Comput Mater Sci 2008;43(3):450–61. http://dx.doi.org/10.1016/j.commatsci.2007.12.016, URL https://www.sciencedirect.com/science/article/pii/S0927025607003515.

[29] Schneider M. The sequential addition and migration method to generate representative volume elements for the homogenization of short fiber reinforced plastics. Comput Mech 2017;59(2):247–63. http://dx.doi.org/10.1007/s00466-016-1350-7, URL https://www.scopus.com/inward/record.uri?eid=2-s2.0-

84994067087&doi=10.1007%2fs00466-016-1350-7&partnerID=40&md5=af1f6ddc05f275e2bc6031edf37a8511. cited By 42.

[30] Tucker III Charles L, Liang Erwin. Stiffness predictions for unidirectional short-fiber composites: Review and evaluation. Composites Sci Technol 1999;59(5):655–71. http://dx.doi.org/10.1016/S0266-3538(98)00120-1, URL https://www.sciencedirect.com/science/article/pii/S0266353898001201.

[31] Giannopoulos GI, Karagiannis D, Anifantis NK. Micromechanical modeling of mechanical behavior of Ti–6Al–4V/TiB composites using FEM analysis. Comput Mater Sci 2007;39(2):437–45. http://dx.doi.org/10.1016/j.commatsci.2006.07.010, URL https://www.sciencedirect.com/science/article/pii/S0927025606002229.

[32] Müller Viktor, Kabel Matthias, Andrä Heiko, Böhlke Thomas. Homogenization of linear elastic properties of short-fiber reinforced composites – A comparison of mean field and voxel-based methods. Int J Solids Struct 2015;67–68:56–70. http://dx.doi.org/10.1016/j.ijsolstr.2015.02.030, URL https://www.sciencedirect.com/science/article/pii/S0020768315000761.

[33] Naili C, Doghri I, Kanit T, Sukiman MS, Aissa-Berraies A, Imad A. Short fiber reinforced composites: Unbiased full-field evaluation of various homogenization methods in elasticity. Composites Sci Technol 2020;187:107942. http://dx.doi.org/10.1016/j.compscitech.2019.107942, URL https://www.sciencedirect.com/science/article/pii/S026635381931961X.

[34] Mentges N, Dashtbozorg B, Mirkhalaf SM. A micromechanics-based artificial neural networks model for elastic properties of short fiber composites. Composites B 2021;213:108736. http://dx.doi.org/10.1016/j.compositesb.2021.108736, URL https://www.sciencedirect.com/science/article/pii/S1359836821001281.

[35] Breuer Kevin, Stommel Markus. Prediction of short fiber composite properties by an artificial neural network trained on an RVE database. Fibers 2021;9(2). http://dx.doi.org/10.3390/fib9020008, URL https://www.mdpi.com/2079-6439/9/2/8.

[36] Doghri I, Tinel L. Micromechanical modeling and computation of elasto-plastic materials reinforced with distributed-orientation fibers. Int J Plast 2005;21(10):1919–40. http://dx.doi.org/10.1016/j.ijplas.2004.09.003.

[37] Kammoun S, Doghri I, Adam L, Robert G, Delannay L. First pseudo-grain failure model for inelastic composites with misaligned short fibers. Composites Part A Appl Sci Manuf 2011;42(12):1892–902. http://dx.doi.org/10.1016/j.compositesa.2011.08.013, URL http://www.sciencedirect.com/science/article/pii/S1359835X11002739.

[38] Advani Suresh G, Tucker Charles L. The use of tensors to describe and predict fiber orientation in short fiber composites. J Rheol 1987;31(8):751–84. http://dx.doi.org/10.1122/1.549945.

[39] Mirkhalaf SM, Eggels EH, van Beurden TJH, Larsson F, Fagerström M. A finite element based orientation averaging method for predicting elastic properties of short fiber reinforced composites. Composites B 2020;202:108388. http://dx.doi.org/10.1016/j.compositesb.2020.108388, URL http://www.sciencedirect.com/science/article/pii/S1359836820334363.

[40] Dafalias YF, Rashid MM. The effect of plastic spin on anisotropic material behavior. Int J Plast 1989;5(3):227–46.

[41] Aravas N. Finite elastoplastic transformations of transversely isotropic metals. Int J Solids Struct 1992;29(17):2137–57.

[42] https://www.e-xstream.com/products/digimat/about-digimat.

[43] Mirkhalaf SM, Pires FM Andrade, Simoes R. Determination of the size of the representative volume element (RVE) for the simulation of heterogeneous polymers at finite strains. Finite Elem Anal Des 2016;119:30–44. http://dx.doi.org/10.1016/j.finel.2016.05.004, URL http://www.sciencedirect.com/science/article/pii/S0168874X16300750.

[44] Modniks J, Andersons J. Modeling the non-linear deformation of a short-flax-fiber-reinforced polymer composite by orientation averaging. Composites B 2013;54(1):188–93. http://dx.doi.org/10.1016/j.compositesb.2013.04.058.

[45] Rabinovitch Oded. An extended high order cohesive interface approach to the debonding analysis of FRP strengthened beams. Int J Mech Sci 2014;81:1–16. http://dx.doi.org/10.1016/j.ijmecsci.2014.01.013, URL https://www.sciencedirect.com/science/article/pii/S0020740314000344.

[46] Kang Ge, Yang Zheng, wan Chen Peng, Liu Rui, jun Ning You, ping Pang Si. Mechanical behavior simulation of particulate-filled composite at meso-scale by numerical manifold method. Int J Mech Sci 2022;213:106846. http://dx.doi.org/10.1016/j.ijmecsci.2021.106846, URL https://www.sciencedirect.com/science/article/pii/S0020740321005683.

[47] Teklal Fatiha, Djebbar Arezki, Allaoui Samir, Hivet Gilles, Joliff Yoann, Kacimi Bachir. A review of analytical models to describe pull-out behavior – Fiber/matrix adhesion. Compos Struct 2018;201:791–815. http://dx.doi.org/10.1016/j.compstruct.2018.06.091, URL https://www.sciencedirect.com/science/article/pii/S0263822317333573.

[48] Cox HL. The elasticity and strength of paper and other fibrous materials. Br J Appl Phys 1952;3(3):72–9. http://dx.doi.org/10.1088/0508-3443/3/3/302, URL https://www.scopus.com/inward/record.uri?eid=2-s2.0-0642356572&doi=10.1088%2f0508-3443%2f3%2f3%2f302&partnerID=40&md5=2d4c62946a7a849c8be544052cf42636. cited By 2785.

[49] Gao X-L, Li K. A shear-lag model for carbon nanotube-reinforced polymer composites. Int J Solids Struct 2005;42(5):1649–67. http://dx.doi.org/10.1016/j.ijsolstr.2004.08.020, URL https://www.sciencedirect.com/science/article/pii/S0020768304004688.

[50] Tsai Jia-Lin, Lu Ting-Chu. Investigating the load transfer efficiency in carbon nanotubes reinforced nanocomposites. Compos Struct 2009;90(2):172–9. http://dx.doi.org/10.1016/j.compstruct.2009.03.004, URL https://www.sciencedirect.com/science/article/pii/S0263822309000713.

[51] Analysis of stress transfer in short fiber-reinforced composites with a partial damage interface by a shear-lag model. Mech Mater 2021;160:103966. http://dx.doi.org/10.1016/j.mechmat.2021.103966, URL https://www.sciencedirect.com/science/article/pii/S0167663621002052.

[52] Rocha DB, de Souza AG, Szostak M, Rosa DDS. Polylactic acid/Lignocellulosic residue composites compatibilized through a starch coating. Polym Compos 2020;41(8):3250–9. http://dx.doi.org/10.1002/pc.25616, URL https://www.scopus.com/inward/record.uri?eid=2-s2.0-85085150486&doi=10.1002%2fpc.25616&partnerID=40&md5=f8746d7db52aafd8f6f2d3835288998a. cited By 1.

[53] Jiang Ning, Li Yaomin, Li Yuankun, Yu Tao, Li Yan, Li Di, Xu Jiachuan, Wang Cuiping, Shi Ying. Effect of short jute fibers on the hydrolytic degradation behavior of poly(lactic acid). Polym Degrad Stab 2020;178:109214. http://dx.doi.org/10.1016/j.polymdegradstab.2020.109214, URL https://www.sciencedirect.com/science/article/pii/S0141391020301464.

[54] Harper LT, Qian C, Turner Ta, Li S, Warrior Na. Representative volume elements for discontinuous carbon fibre composites – Part 2: Determining the critical size. Composites Sci Technol 2012;72(2):204–10. http://dx.doi.org/10.1016/j.compscitech.2011.11.003, URL http://linkinghub.elsevier.com/retrieve/pii/S0266353811003848.

[55] Kari S, Berger H, Gabbert U. Numerical evaluation of effective material properties of randomly distributed short cylindrical fibre composites. Comput Mater Sci 2007;39(1):198–204. http://dx.doi.org/10.1016/j.commatsci.2006.02.024.

[56] Qi Lehua, Chao Xujiang, Tian Wenlong, Ma Wenjing, Li Hejun. Numerical study of the effects of irregular pores on transverse mechanical properties of unidirectional composites. Composites Sci Technol 2018;159:142–51. http://dx.doi.org/10.1016/j.compscitech.2018.02.020, URL http://www.sciencedirect.com/science/article/pii/S0266353817311090.